https://doi.org/10.5194/bg-2022-134
Preprint. Discussion started: 20 June 2022

Biogeosciences Discussions

Observation-constrained estimates of the global ocean carbon sink from Earth System Models

Jens Terhaar[1,2], Thomas L. Frölicher[1,2], Fortunat Joos[1,2]

[1]Climate and Environmental Physics, Physics Institute, University of Bern, Switzerland
[2]Oeschger Centre for Climate Change Research, University of Bern, Switzerland

Correspondence to: Jens Terhaar (jens.terhaar@unibe.ch)

Abstract. The ocean slows global warming by currently taking up around one quarter of all human-made CO_2 emissions. However, estimates of the ocean anthropogenic carbon uptake vary across various observation-based and model-based approaches. Here, we show that the global ocean anthropogenic carbon sink simulated by Earth System Models can be constrained by two physical parameters, the present-day sea surface salinity in the subtropical-polar frontal zone in the Southern Ocean and the strength of the Atlantic Meridional Overturning Circulation, and one biogeochemical parameter, the Revelle factor of the global surface ocean. By exploiting this three-dimensional emergent constraint with observations, we provide a new model- and observation-based estimate of the past, present and future global ocean anthropogenic carbon sink and show that the ocean carbon sink is 9-11% larger than previously estimated. Furthermore, the constraint reduces uncertainties of the past and present global ocean anthropogenic carbon sink by 42-59% and the future sink by 32-62% depending on the scenario, allowing for a better understanding of the global carbon cycle and better targeted climate and ocean policies. The here identified key parameters for the ocean carbon sink should be quantified when presenting simulated ocean anthropogenic carbon uptake as in the Global Carbon Budget and be used to adjust these simulated estimates if necessary. The larger ocean sink results in enhanced ocean acidification over the 21st century, which further threatens marine ecosystems by reducing the water volume that is projected to be undersaturated towards aragonite by around 3.7-7.4 million km^3 more than originally projected.

1 Introduction

The emissions of anthropogenic CO_2 (C_{ant}) since the beginning of industrialization through fossil-fuel burning, cement production and land-use change have altered the global carbon cycle and climate (Friedlingstein et al., 2022). Around 40% of the additional carbon since 1850 has accumulated in the atmosphere, where it represents the main anthropogenic greenhouse gas (IPCC, 2021). More than half of the emitted C_{ant} has been taken up by the land biosphere (~30%) and the ocean (~25%) (Friedlingstein et al., 2022). The remaining ~5% are the budget imbalance, a mismatch between carbon emissions and sink

https://doi.org/10.5194/bg-2022-134
Preprint. Discussion started: 20 June 2022

estimates which cannot be explained yet (Friedlingstein et al., 2022). By taking up each around a quarter of the C_{ant} emissions, the land biosphere and ocean sinks slow down global warming and climate change.

The ocean C_{ant} sink is defined here as a combination of the uptake of newly emitted carbon and the change in the natural carbon inventory in the ocean due to changes in temperatures, winds, and the freshwater cycle caused by climate change (Joos et al., 1999; Frölicher and Joos, 2010; McNeil and Matear, 2013). The uptake rate of C_{ant} on sub-millennial timescales is determined by the ocean circulation, carbonate chemistry, and biology (Sarmiento et al., 1998; Joos et al., 1999; Caldeira and Duffy, 2000; Sabine et al., 2004; Hauck and Völker, 2015). The rate limiting process is circulation that transports surface waters with high C_{ant} concentrations into the deeper ocean and allows waters with low or no C_{ant} concentrations to upwell back to the ocean surface. The largest part of this ocean upwelling occurs in the Southern Ocean where strong westerlies drive northward Ekman transport of surface waters, which are then replaced by older, deeper water masses (Marshall and Speer, 2012; Talley, 2013; Morrison et al., 2015). These predominantly northward flowing waters take up C_{ant} from the atmosphere and are eventually transferred to mode and intermediate waters that sink back into the ocean interior (Marshall and Speer, 2012; Talley, 2013). This overturning makes the Southern Ocean the largest marine C_{ant} sink (~40% of global ocean C_{ant} uptake) (Caldeira and Duffy, 2000; Mikaloff Fletcher et al., 2006; Gerber et al., 2009; Gruber et al., 2009; Frölicher et al., 2015; Terhaar et al., 2021b). Another region of large uptake rates is the North Atlantic (Caldeira and Duffy, 2000; Mikaloff Fletcher et al., 2006; Gruber et al., 2009; Goris et al., 2018), where the Atlantic Meridional Overturning Circulation (AMOC) transports surface waters with high C_{ant} (Pérez et al., 2013) and subsurface waters with low C_{ant} concentrations northward (Ridge and McKinley, 2020). The subsurface waters outcrop in the subpolar North Atlantic where they take up C_{ant} from the atmosphere (Ridge and McKinley, 2020). These high C_{ant} waters are then subducted by the AMOC into the deep ocean where the C_{ant} is efficiently stored (Joos et al., 1999; Winton et al., 2013). While the circulation determines the volume that is transported into the deeper ocean, the Revelle factor (Revelle and Suess, 1957; Sabine et al., 2004) determines the concentration of C_{ant} in these water masses. The Revelle factor describes the biogeochemical capacity of the ocean to take up C_{ant}. In addition to the circulation and marine chemistry, biology also modulates the global ocean C_{ant} uptake through changes in the net primary production and export fluxes of organic matter and biogenic particles from the surface ocean to the interior ocean (Riebesell et al., 2007;

https://doi.org/10.5194/bg-2022-134
Preprint. Discussion started: 20 June 2022

Hauck and Völker, 2015) and in the remineralization or dissolution of organic matter and biogenic material at depth (Bendtsen et al., 2002; Gangstø et al., 2008; Kwon et al., 2009; Roth et al., 2014). However, the contribution of biology to C_{ant} uptake is estimated to be relatively small compared to the impact of circulation and the Revelle factor(Sarmiento and Sundquist, 1992; Sarmiento et al., 1992; Joos et al., 1999; Plattner et al., 2001; Frölicher and Joos, 2010; Terhaar et al., 2019; Canadell et al., 2021), despite its overall importance for natural carbon fluxes (Falkowski et al., 1998; Steinacher et al., 2010).

In addition to slowing global warming, the C_{ant} uptake by the ocean also causes ocean acidification (Orr et al., 2005; Gattuso and Hansson, 2011; Kwiatkowski et al., 2020), i.e., a decline in ocean pH and carbonate ion concentrations. The decline in carbonate ion concentrations has negative effects on the growth and survival of many marine species, especially on calcifying organisms whose shells and skeletons are made up of calcium carbonate minerals (Orr et al., 2005; Fabry et al., 2008; Kroeker et al., 2010, 2013; Doney et al., 2020). Calcium carbonate minerals in the ocean exists mainly in its metastable forms of aragonite and high-magnesium calcite and its more stable form calcite. The stability of calcium carbonate minerals is described by their saturation states (Ω), which describe the product of the concentrations of calcium ($[Ca^{2+}]$) and carbonate ions ($[CO_3^{2-}]$) divided by their product in equilibrium. Reductions of saturation states of aragonite (Ω_{arag}) and calcite (Ω_{calc}) have shown to negatively impact organisms and ecosystems (Langdon and Atkinson, 2005; Kroeker et al., 2010; Bednaršek et al., 2014; Albright et al., 2016). Once, saturation states drop below one, the water is undersaturated and actively corrosive towards the respective mineral form.

Accurately quantifying the ocean anthropogenic carbon sink is thus of crucial importance for understanding and quantifying the carbon cycle, global warming and climate change, as well as ocean acidification. A better knowledge of the size of the historical and future ocean carbon sink and reduced uncertainties will hence not only lead to an improved understanding of the overall carbon cycle and global climate change (IPCC, 2021), but also allow targeted climate and ocean policies (IPCC, 2022). One of the key tools to assess the past, present, and future ocean carbon sink are Earth System Models (ESMs). However, the simulated ocean C_{ant} sink varies across the different ESMs (Frölicher et al., 2015; Wang et al., 2016; Bronselaer et al., 2017; Terhaar et al., 2021b) and the model differences grow over time, i.e., ESMs that simulate a small ocean C_{ant} uptake over the

https://doi.org/10.5194/bg-2022-134
Preprint. Discussion started: 20 June 2022

Biogeosciences Discussions Open Access EGU

last decades also simulate a small uptake over the 21st century (Figure 1b) (Wang et al., 2016). Therefore, a better knowledge of the ocean C_{ant} sink in the last decades would be one possibility to reduce uncertainties in the simulated ocean carbon from 1850 to 2100.

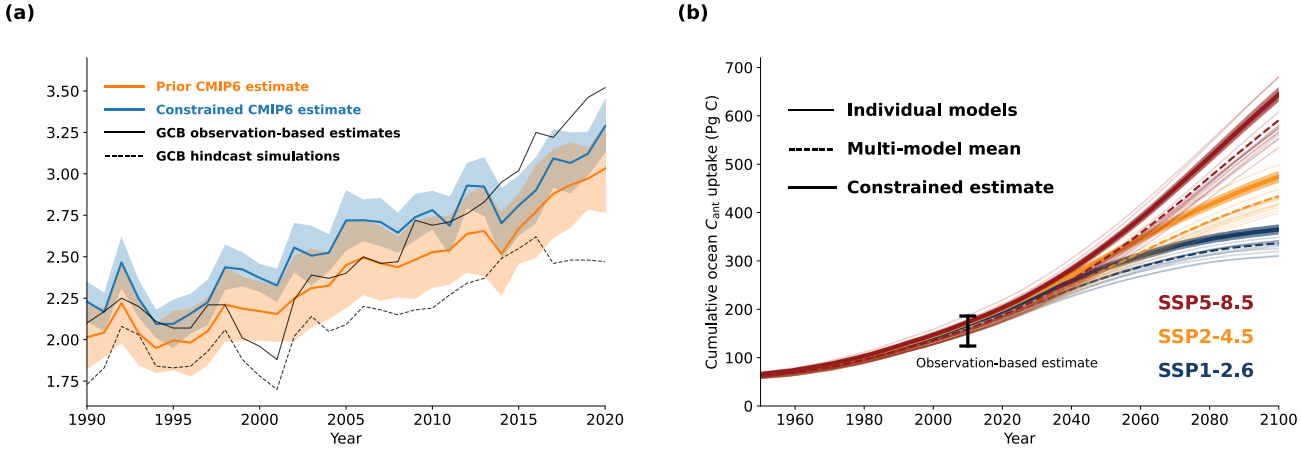

Figure 1. Simulated ocean anthropogenic carbon uptake from Earth System Models. (a) Simulated annual mean air-sea C_{ant} fluxes from 17 CMIP6 Earth System Models from 1995 to 2020 before (orange line) and after the constraint is applied (blue line). After 2014, results from SSP5-8.5 were chosen as this is the only SSP for which each model provided results and differences in atmospheric CO_2 mixing ratios in SSP5-8.5 (Meinshausen et al., 2020) are small compared to observations (Trends in Atmospheric Carbon Dioxide (NOAA/GML)) until 2020 (maximum difference of 2.5 ppm in 2020). In addition, mean air-sea C_{ant} fluxes based on multiple observation-based estimates (black solid line) and hindcast simulations (black dashed line) from the Global Carbon Budget 2021 (Friedlingstein et al., 2022) are shown. For readability, the uncertainties of these estimates (on average 0.24 Pg C yr^{-1} for observation-based estimates and 0.28 Pg C yr^{-1} for hindcast simulations) are not shown in the figure. **(b)** Simulated cumulative ocean C_{ant} uptake since 1765 for the historic period until 2014 (17 ESMs) and for the future from 2015 to 2100 under SSP1-2.6 (blue, 14 ESMs), SSP2-4.5 (orange, 16 ESMs), and SSP5-8.5 (red, 17 ESMs). Thin lines show the results from each individual ESM, the dashed lines the multi-model mean, the solid lines the constrained estimate, and the shading the uncertainty around the constrained estimate. As ESM simulations in CMIP6 start in 1850, the air-sea C_{ant} fluxes were corrected upwards for the late starting date following Bronselaer et al. (2017) (see Appendix A.1). Furthermore, the observation-based ocean C_{ant} inventory estimate in 2010 from Khatiwala et al. (2013) is shown.

2 Quantifying the past ocean anthropogenic carbon sink with observations and hindcast simulations and existing uncertainties

The large background concentration of dissolved inorganic carbon (C_T) in the ocean and the vast ocean volume make it difficult to directly observe the relatively small anthropogenic perturbations in the ocean interior. Therefore, different methods have been developed to estimate the accumulation of anthropogenic carbon (C_{ant}) in the ocean (Khatiwala et al., 2013), such as the

https://doi.org/10.5194/bg-2022-134
Preprint. Discussion started: 20 June 2022

100 ΔC* method (Gruber et al., 1996; Sabine et al., 2004) or the Transient Time Distribution method (Hall et al., 2002) based on observations of inert tracers, like CFCs. These estimates result in an estimated ocean C_{ant} inventory in 2010 of 155±31 Pg C (Khatiwala et al., 2013) (Figure 1b, Table 1), but do not or only partly include climate-driven changes in C_T.

Further development of the ΔC* method into the eMLR(C*) method (Clement and Gruber, 2018) and more observations
105 through new techniques, such as (Bio-)ARGO-floats (Claustre et al., 2020), and more research cruises (Lauvset et al., 2021) allowed to quantify the increase in marine C_{ant} on shorter timescales and with reduced uncertainty. The so-estimated increase in C_{ant} from 1994 to 2007 is 34±4 Pg C (12% uncertainty, Table 1) (Gruber et al., 2019a), again not accounting for potential climate-driven changes in C_T. In addition to interior C_{ant} estimates, surface ocean observations of the partial pressure of CO_2 (pCO_2) and new statistical methods, such as neural networks (Landschützer et al., 2016), have allowed to establish observation-
110 based estimates of the air-sea CO_2 flux (Rödenbeck et al., 2014; Zeng et al., 2014; Landschützer et al., 2016; Gregor et al., 2019; Watson et al., 2020; Iida et al., 2021; Gregor and Gruber, 2021; Chau et al., 2022). When subtracting the pre-industrial outflux of CO_2 due to riverine carbon fluxes (Sarmiento and Sundquist, 1992; Aumont et al., 2001; Jacobson et al., 2007; Resplandy et al., 2018; Lacroix et al., 2020; Regnier et al., 2022) from these air-sea CO_2 flux estimates, the global ocean C_{ant} uptake can be derived (Friedlingstein et al., 2022), resulting in an estimated ocean C_{ant} uptake from 1994 to 2007 of 29±4 Pg
115 C (14% uncertainty, Table 1). The difference of 5 Pg C between the interior and surface ocean mean estimates was attributed to outgassing of ocean CO_2 caused by a changing climate (Gruber et al., 2019a). However, simulations from ESMs of the sixth phase of the Coupled Model Intercomparison Project (CMIP6) estimate this climate-driven air-sea CO_2 flux from 1994 to 2007 to be -1.6±0.5 Pg C (Table A.1.3), significantly smaller than the previously assumed flux of -5 Pg C (Gruber et al., 2019a), leaving an unexplained difference between both observation-based products although their uncertainty ranges overlap.

120

https://doi.org/10.5194/bg-2022-134
Preprint. Discussion started: 20 June 2022

Table 1. Global ocean air-sea C_{ant} flux estimates based on 17 ESMs from CMIP6 before and after constraint as well as previous estimates over different time periods. Prior uncertainty is the multi-model standard deviation. The uncertainty of the starting date corrected values also includes the uncertainty from that correction. The constrained uncertainty is a combination of the starting date correction, the multi-model standard deviation after the constraint is applied, and the uncertainty from the correction itself (see Appendices A.1 and A3). Uncertainties from the decadal variability on shorter timescales, e.g., for 1994-2007, are not included. The star indicates estimates that do not account for climate-driven changes in the ocean carbon sink.

Period	Cumulative air-sea C_{ant} flux (Pg C)					
	CMIP6			Global Carbon Budget 2021 (Friedlingstein et al., 2022)	Others	
	Prior	Starting date corrected	Constrained	observation-based / hindcast simulations	Estimate	Source
1994-2007	26.8 ± 2.1	28.8 ± 2.2	31.5 ± 0.9	29 ± 4 / 26 ±3	34 ± 4*	(Gruber et al., 2019a)
1765-2010		164 ± 12	177 ± 7		155 ± 31*	(Khatiwala et al., 2013)
1850-2014	138 ± 10	157 ± 12	171 ± 6	150 ± 30		
1960-2020	106 ± 8	117 ± 9	128 ± 4	115 ± 25		
1850-2020	154 ± 11	174 ± 13	189 ± 7	170 ± 35		
2020-2100 (SSP1-2.6)	150 ± 11	156 ± 11	173 ± 8			
2020-2100 (SSP2-4.5)	244 ± 16	251 ± 17	277 ± 9			
2020-2100 (SSP5-8.5)	399 ± 29	407 ± 30	445 ± 12			

https://doi.org/10.5194/bg-2022-134
Preprint. Discussion started: 20 June 2022

An alternative way of estimating the strength of the ocean carbon sink is the use of global ocean biogeochemical models forced with atmospheric reanalysis data (Sarmiento et al., 1992; Friedlingstein et al., 2022). From 1994 to 2007, the ocean biogeochemical hindcast models that participated in the Global Carbon Budget 2021 (Friedlingstein et al., 2022) simulate a C_{ant} uptake of 26±3 Pg C (Table 1). This estimate is 3 Pg C below the surface observation-based estimate and the difference increases further after 2010 (Figure 1a). Compared to the interior ocean C_{ant} estimate, the simulated uptake by these hindcast models is 3-6 Pg C (10-19%) smaller depending on the correction term that is used for climate change induced outgassing of natural CO_2. Such differences between observation-based and simulated ocean C_{ant} uptake could be explained regionally by systematic biases in models (Goris et al., 2018; Terhaar et al., 2020a, 2021a, b), as well as data sparsity (Bushinsky et al., 2019; Gloege et al., 2021).

Overall, the difference between ocean hindcast models, observation-based CO_2 flux estimates, and interior ocean C_{ant} estimates as well as the uncertainties in the climate-driven change in C_T and pre-industrial outgassing indicate that uncertainties of the past ocean C_{ant} sink remain larger than the uncertainties of these individual products (Crisp et al., 2022) and do not allow to constrain the ocean C_{ant} sink.

3 Constraining the ocean anthropogenic carbon sink in Earth System Models

Another way to constrain the present and future global ocean anthropogenic carbon sink is the use of process-based emergent constraints (Orr, 2002) that identify a relationship across an ensemble of ESMs between a relatively uncertain variable, such as the C_{ant} uptake in the Southern Ocean, and a variable that can be observed with a relatively small uncertainty, such as the sea surface salinity in the subtropical-polar frontal zone in the Southern Ocean. The identified relationship is then combined with observations, in this example the sea surface salinity, to better estimate the uncertain variable, here the C_{ant} uptake in the Southern Ocean (Terhaar et al., 2021b). Such relationships must be explainable by an underlying mechanism (Hall et al., 2019), i.e., higher sea surface salinity in the frontal zone leads to denser sea surface waters and stronger mode and intermediate water formation, which enhances the transport of C_{ant} from the ocean surface to the ocean interior and allows hence for more C_{ant} uptake. In recent years, process-based emergent constraints (Orr, 2002; Matsumoto et al., 2004; Wenzel et al., 2014;

https://doi.org/10.5194/bg-2022-134
Preprint. Discussion started: 20 June 2022

Kwiatkowski et al., 2017; Goris et al., 2018; Eyring et al., 2019; Hall et al., 2019; Terhaar et al., 2020a, 2021a, b) have successfully reduced uncertainties in simulated processes across ensembles of ESMs. In the ocean, for example, a bias towards too little C_{ant} uptake was identified in the Southern Ocean (Terhaar et al., 2021b). Similarly, ESMs from CMIP5 were shown to underestimate the future uptake of C_{ant} in the North Atlantic due to too little sequestration of C_{ant} into the deeper ocean (Goris et al., 2018). However, the relatively uncertain observation-based estimates of C_{ant} sequestration (see section above) did not allow to reduce uncertainties. Despite a better understanding of the regional C_{ant} uptake, uncertainties of the global ocean C_{ant} sink could not yet been reduced.

Here, we identify a mechanistic constraint for the global ocean C_{ant} sink across 17 ESMs from CMIP6 (Table A.1.1). We demonstrate that a linear combination of three observable quantities, (1) the sea surface salinity in the subtropical-polar frontal zone in the Southern Ocean, (2) the strength of the AMOC at 26.5°N, and (3) the globally averaged surface ocean Revelle factor, can successfully predict the strength of the global ocean C_{ant} sink across the CMIP6 ESMs (r^2 of 0.87 for the global ocean C_{ant} uptake from 1994 to 2007). The sea surface salinity in the subtropical-polar frontal zone in the Southern Ocean and the AMOC determine the strength of the two most important regions of mode, intermediate, and deep-water formation (Marshall and Speer, 2012; Talley, 2013; Buckley and Marshall, 2016; McCarthy et al., 2020). In addition, the Revelle factor accounts for biases in the biogeochemical buffer capacity of the ocean, i.e., the relative increase in ocean C_T for a given relative increase in ocean pCO_2 (Revelle and Suess, 1957). As the Revelle factor quantifies relative increases in ocean C_T, the increase in surface ocean C_{ant} depends on the Revelle factor and the natural surface ocean C_T. Therefore, the Revelle factor in the ESMs was adjusted for model biases in natural surface ocean C_T (see Appendix A.1). Compared to observations, CMIP6 models represent the observation-based average strength of the AMOC from 2004 to 2020 (16.91 ± 0.49 Sv) (McCarthy et al., 2020) right but have a large inter-model spread (16.91 ± 3.00 Sv), underestimate the observed inter-frontal sea surface salinity (34.07 ± 0.02) and have a large inter-model spread (33.89 ± 0.13), and overestimate the surface-averaged Revelle factor that was derived by GLODAPv2 (10.45 ± 0.01) by 0.24 (10.73 ± 0.24) with largest Revelle factor biases in the main C_{ant} uptake regions (Figure 2). The underestimation of the C_T-adjusted Revelle factor by the ESM ensemble is mainly due to a bias towards too

https://doi.org/10.5194/bg-2022-134
Preprint. Discussion started: 20 June 2022

small concentrations of surface ocean carbonate ion concentrations (Sarmiento et al., 1995), caused by a too small difference of surface ocean alkalinity and C_T (Figure A.1.2).

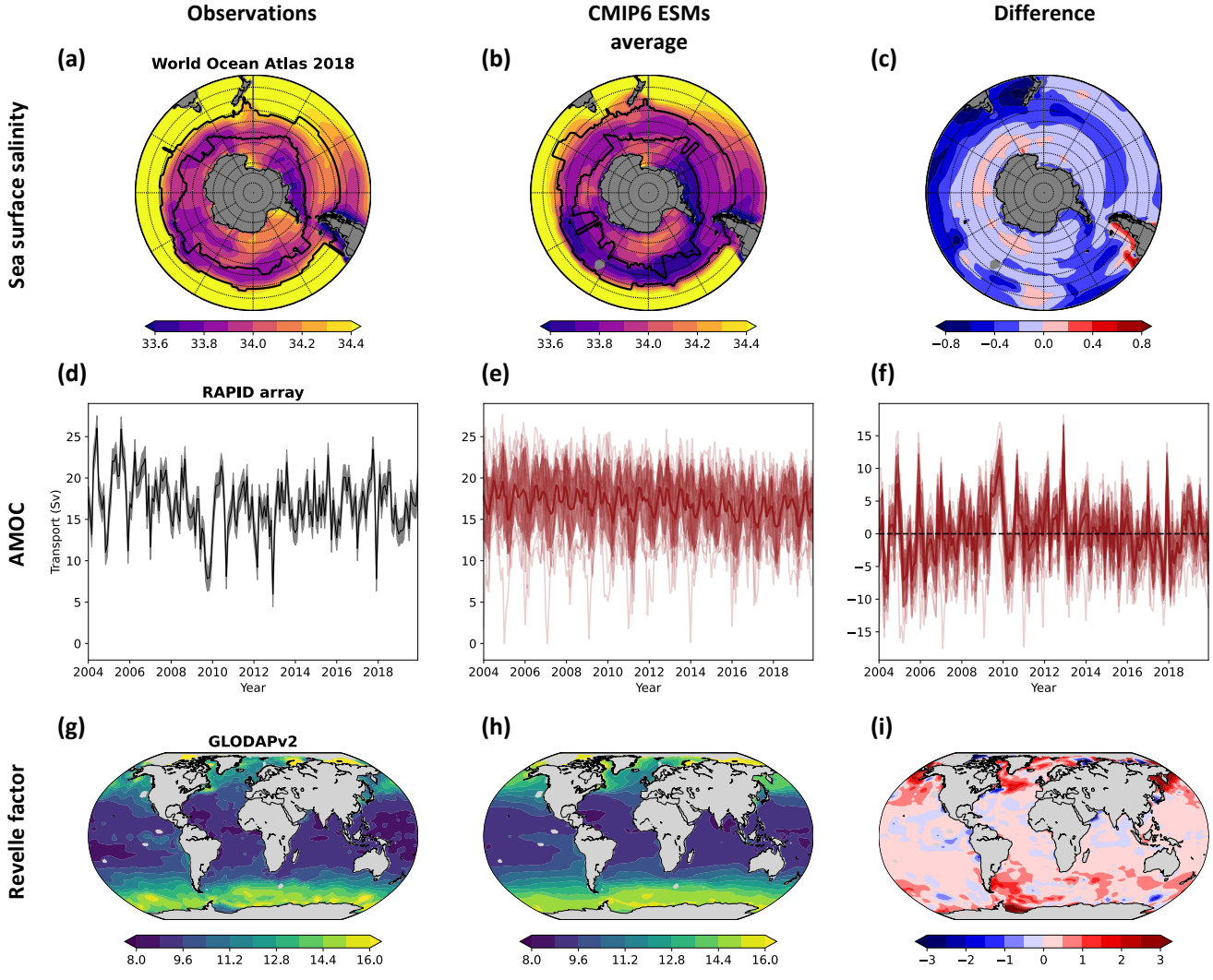

Figure 2. Sea surface salinity in the Southern Ocean, the Atlantic Meridional Overturning Circulation, and the Revelle factor at the ocean surface from observations and Earth System Models. Annual mean sea surface salinity from the **(a)** World Ocean Atlas 2018 (Zweng et al., 2018; Locarnini et al., 2018), **(b)** 17 Earth System Models from CMIP6 from 1995 to 2014, and **(c)** the difference between both. The black lines in **(a,b)** indicate the annual mean positions of the Polar and Subtropical Fronts. The monthly-averaged Atlantic Meridional Overturning Circulation, here defined as the maximum of the streamfunction at 26.5°N, from 2004 to 2020 as **(d)** observed by the RAPID array (McCarthy et al., 2020), **(e)** as simulated by 17 Earth System Models from CMIP6, and **(f)** the difference between both.

https://doi.org/10.5194/bg-2022-134
Preprint. Discussion started: 20 June 2022

Each model simulation is shown in **(e)** and **(f)** as a thin red line, the multi-model average is shown as a thick red line, and the multi-model standard deviation is shown as red shading. The annual mean sea surface Revelle factor calculated with *mocsy2.0* (Orr and Epitalon, 2015) from **(g)** gridded GLODAPv2 observations that are normalized to the year 2002 (Lauvset et al., 2016), from **(h)** output of 17 Earth System Model simulations from CMIP6 in 2002 and adjusted for biases in the surface ocean C_T (see Appendix A.1), and **(i)** their difference.

By exploiting this multi-variable emergent constraint with observations, the simulated C_{ant} uptake by ESMs from 1994 to 2007 increases from 28.8 ± 2.2 Pg C to 31.5 ± 0.9 Pg C (Figures 1 & 3, Tables 1 & A.1.2). Biases in the Southern Ocean salinity are responsible for around 60% of the bias in the global ocean C_{ant} uptake in the CMIP6 models while the bias in the Revelle factor explains the remaining 40% (Figure 3). The AMOC, whose multi-model mean in ESMs is similar to observations, does not change the central C_{ant} uptake estimate but allows to reduce uncertainties (Figure 3). The constrained C_{ant} uptake is 0.5 Pg C smaller than the interior ocean C_{ant} estimate based on observations (Gruber et al., 2019a) when subtracting the multi-model mean climate-driven CO_2 flux estimate from the CMIP6 models (Table A.1.3) and 2.5 Pg C larger than the observation-based air-sea C_{ant} flux estimates from 1994 to 2007. However, after 2013 the observation-based air-sea C_{ant} flux estimates become slightly larger than the constrained CMIP6 ESM estimates (Figure 1). Thus, the mismatch between observation-based air-sea C_{ant} flux estimates from 1994 to 2007 and the here provided results may not exist over a longer period of time and be caused by a different timing and magnitude of decadal variabilities in ESMs and the real world (Landschützer et al., 2016; Gruber et al., 2019b; Bennington et al., 2022), as well as uncertainties in the observation-based products (Bushinsky et al., 2019; Gloege et al., 2021, 2022).

https://doi.org/10.5194/bg-2022-134
Preprint. Discussion started: 20 June 2022

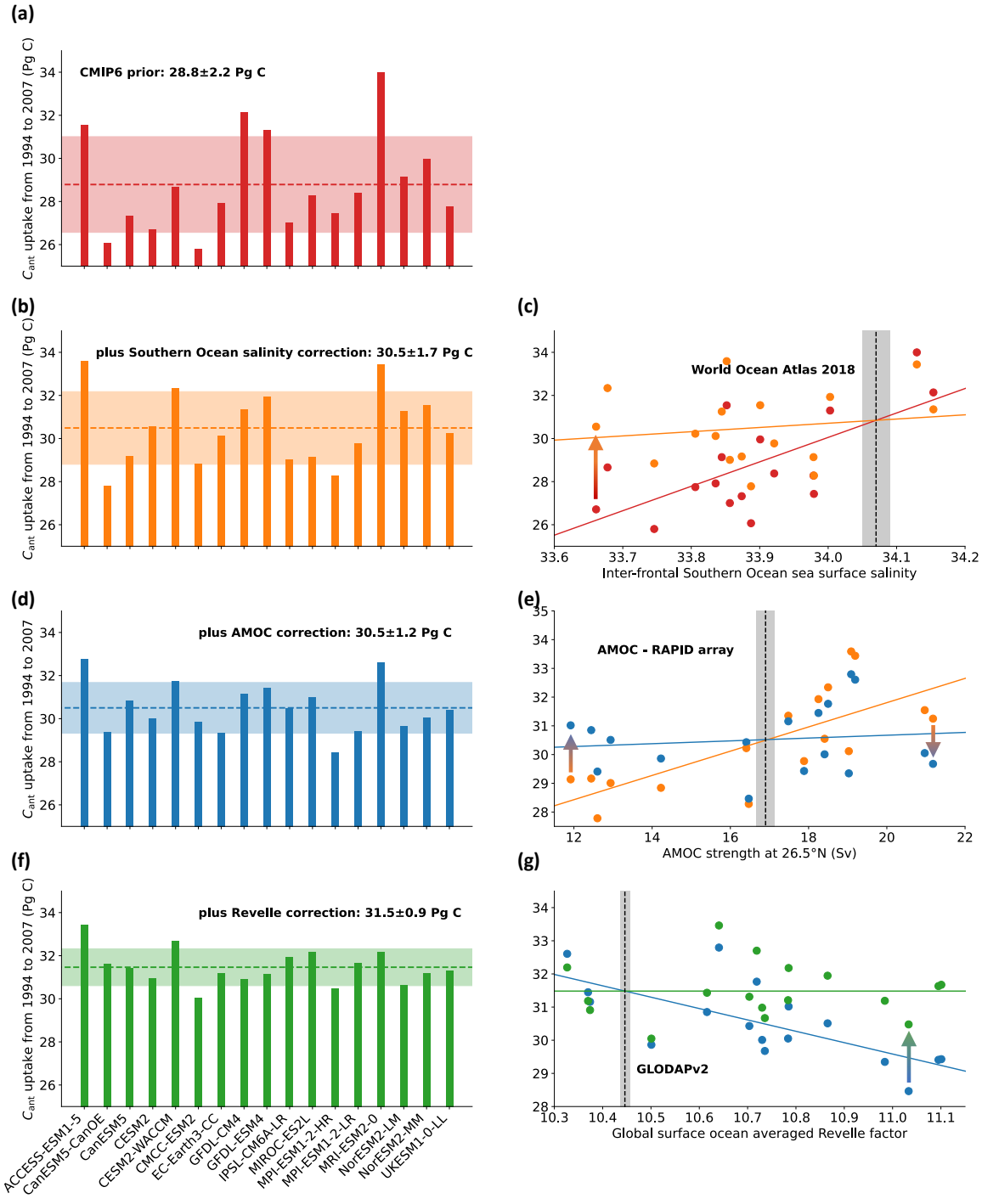

Figure 3. Global ocean anthropogenic carbon simulated by Earth System Models from CMIP6 corrected for biases in sea surface salinity in the Southern Ocean, the Atlantic Meridional Overturning Circulation, and the Revelle factor. (a) Global ocean

https://doi.org/10.5194/bg-2022-134
Preprint. Discussion started: 20 June 2022

anthropogenic carbon (C_{ant}) uptake from 1994 to 2007 as simulated by 17 ESMs from CMIP6 and corrected for the late starting date (Bronselaer et al., 2017). In the years 1994 and 2007, only half of the annual C_{ant} uptake was accounted for to make it comparable to interior ocean estimates that compare changes in C_{ant} from mid 1994 to mid 2007 and not from the start of 1994 to the end of 2007 (Gruber et al., 2019a). **(b)** C_{ant} uptake after correcting the simulated C_{ant} uptake from **(a)** for biases in the Southern Ocean Sea surface salinity (Terhaar et al., 2021b) from **(c)**. The dots in **(c)** represent individual models before (red) and after (orange) the sea surface salinity correction. **(d)** C_{ant} uptake after correcting sea surface salinity corrected C_{ant} uptake from **(b)** for biases in the Atlantic Meridional Overturning Circulation from **(e)**. The dots in **(e)** represent individual models before (orange) and after (blue) the Atlantic Meridional Overturning Circulation correction. **(f)** C_{ant} uptake after correcting the sea surface salinity and Atlantic Meridional Overturning Circulation corrected C_{ant} uptake from **(d)** for biases in the global ocean surface Revelle factor from **(g)**. The dots in **(g)** represent individual models before (blue) and after (green) the Revelle factor correction. The simulated Revelle factor by the ESMs was adjusted for biases in the surface ocean C_T (see Appendix A.1). The dashed coloured lines in **(a)**, **(b)**, **(d)**, **(f)** show the multi-model mean and the shading shows the uncertainty, which is a combination of the multi-model standard deviation after correction and the uncertainty of the correction factor due to the uncertainty of the observational constraint (see Appendix A.1). The dashed black lines in **(c)**, **(e)**, **(g)** show the observations from the World Ocean Atlas 2018 (Zweng et al., 2018; Locarnini et al., 2018), the RAPID array (McCarthy et al., 2020), and GLODAPv2 (Lauvset et al., 2016) with their uncertainties as grey shading, the coloured lines show linear fits, and the arrows illustrate the correction for individual models.

Both, the unconstrained and constrained ESM estimates, are larger than the hindcast simulation estimates and uptake in ESMs does not stop to grow after 2015 as it does in the hindcast simulations. The combination of interior ocean C_{ant} estimates, air-sea CO_2 flux-based C_{ant} uptake estimates, and simulated C_{ant} uptake by ESMs estimates suggests that the hindcast simulations underestimate the ocean C_{ant} uptake and that the Global Carbon Budget 2021 estimate of the ocean C_{ant} uptake over the last decades should hence be corrected upwards. Reasons for this underestimation may be an underestimation of the AMOC or the Southern Ocean inter-frontal sea surface salinity, an overestimation of the Revelle factor, a too small ensemble of models (8 models) that is biased towards low uptake models, too short spin-up times (Séférian et al., 2016), or different pre-industrial atmospheric CO_2 mixing ratios (Bronselaer et al., 2017; Friedlingstein et al., 2022). However, even after correcting these hindcast simulations upwards by employing the here identified emergent constraint, their corrected estimate may remain below the CMIP-derived estimate here due to the historical decadal variations in the C_{ant} uptake that is not represented in fully coupled ESMs (Landschützer et al., 2016; Gruber et al., 2019b; Bennington et al., 2022). A detailed analysis by the individual modelling teams would be necessary to identify the reason for underestimation in the individual hindcast models.

https://doi.org/10.5194/bg-2022-134
Preprint. Discussion started: 20 June 2022

Over the historical period from 1850 to 2020, the here identified constraint increases the simulated ocean C_{ant} uptake by 15 Pg C ($r^2 = 0.80$) from 174 ± 13 Pg C to 189 ± 7 Pg C (Table 1). The constrained estimate of the C_{ant} agrees within the uncertainties with the estimate from the Global Carbon Budget for the same period (170±35 Pg C) (Friedlingstein et al., 2022), which is a combination of prognostic approaches until 1959 (Khatiwala et al., 2013; DeVries, 2014), and ocean hindcast simulations and observation-based CO_2 flux products from 1960 to 2020 (Friedlingstein et al., 2022). However, our new estimate is 19 Pg C larger and could explain around three quarters of the budget imbalance (B_{IM}) between global CO_2 emissions and sinks over this period (25 Pg C) (Friedlingstein et al., 2022) and contribute to answering an important outstanding question in the carbon cycle community.

Overall, this new estimate of the ocean C_{ant} uptake, based on ESMs and constrained by observations, presents hence an independent and new estimate of the past and present ocean C_{ant} uptake that is 42-59% less uncertain and around 10% larger than the multi-model average and standard deviation. The lower bound of the uncertainty correction is for the past ocean C_{ant} uptake since 1765 where the late-starting date correction introduces an uncertainty that cannot be reduced without running the simulations from 1765 onwards. Towards the end of the 20th century, the uncertainty from this correction becomes smaller so that the emergent constraint can reduce uncertainties by almost 60%.

4 Consequences for projected ocean anthropogenic carbon uptake and acidification over the 21st century

As the present and future C_{ant} uptake are strongly correlated across ESMs, the here identified relationship can also be used to constrain future projections of the global ocean C_{ant} uptake. The global ocean C_{ant} uptake from 2020 to 2100 increases from 156 ± 11 Pg C to 173 ± 8 Pg C (r^2=0.56) under the high-mitigation low emissions Shared Socioeconomic Pathway 1-2.6 (SSP1-2.6) that likely allows to keep global warming below 2°C (O'Neill et al., 2016; Riahi et al., 2017), from 251 ± 17 Pg C to 277 ± 9 Pg C (r^2=0.74) under the middle-of-the-road SSP2-4.5, and from 407 ± 30 Pg C to 445 ± 12 Pg C (r^2=0.87) under the high-emissions no mitigation SSP5-8.5 (Figure 1b). Overall, the future ocean C_{ant} uptake in CMIP6 models is thus 9-11% larger than simulated by ESMs and 32-62% less uncertain depending on the future scenario. The correlation coefficient and hence the uncertainty reduction reduces, but remains still large, when atmospheric CO_2 stops to increase (SSP1-2.6, SSP2-4.5).

https://doi.org/10.5194/bg-2022-134
Preprint. Discussion started: 20 June 2022

Larger uncertainties for stabilization than for near-exponential growth scenarios are expected as the reversal of the atmospheric CO_2 growth rate will exert a stronger external impact on the magnitude of the ocean carbon sink (McKinley et al., 2020).

The increase in projected uptake of C_{ant} also increases the estimate of future ocean acidification rate. For ocean ecosystems, the threshold for water masses become undersaturated towards specific calcium carbonate minerals (Ω=1) is of critical importance (Orr et al., 2005; Fabry et al., 2008; Doney et al., 2020), although negative effects for some calcifying organisms can already be observed at saturation states above one (Ries et al., 2009) and some calcifying organisms can even live in undersaturated waters (Lebrato et al., 2016). Over the 21st century, the volume of water masses in the global ocean that remain supersaturated towards the meta-stable calcium carbonate mineral aragonite is projected to decrease in CMIP6 from 283 million km^3 in 2002 (based on GLODAPv2 observations (Lauvset et al., 2016)) to 194±6 million km^3 under SSP1-2.6, to 143±4 million km^3 under SSP2-4.5, and to 97±4 million km^3 under SSP5-8.5. The constraint reduces these estimates to 186±5, 138±2, and 93±2 million km^3 respectively (r^2=0.31-0.69), resulting in an additional decrease of the available habitat for calcifying organisms of 3.7-7.4 million km^3 depending on the scenario. This additionally projected habitat loss is mainly located in the mesopelagic layer between 200 and 1000 m and affects thus organisms that live their permanently or temporarily during diel vertical migration (Behrenfeld et al., 2019). The additionally undersaturated volume corresponds to an area of 1.6-3.1 times the area of the Mediterranean Sea whose mesopelagic layer would be additionally undersaturated towards aragonite. However, the global character of the constraint and the uncertainty of the interior distribution of C_{ant} do not allow to localise these areas.

5 Robustness of the emergent constraint and possible impact of changing riverine carbon input over time

Emergent constraints across large datasets such as an ensemble of ESMs with hundreds of variables can always be found and might not necessarily be reliable and robust (Caldwell et al., 2014; Brient, 2020; Sanderson et al., 2021; Williamson et al., 2021). To test the robustness of emergent constraints, three criteria were proposed (Hall et al., 2019). The constraint must be relying on well understood mechanisms, that mechanism must be reliable, and the constraint must be validated in an independent model ensemble. Here, the well understood mechanisms are the fundamental ocean biogeochemical properties

https://doi.org/10.5194/bg-2022-134
Preprint. Discussion started: 20 June 2022

such as the Revelle factor (Revelle and Suess, 1957), as well as the Southern Ocean and North Atlantic large-scale ocean circulation features that are known to be the determining factors for the ocean ventilation (Marshall and Speer, 2012; Talley, 2013; Buckley and Marshall, 2016). For the Southern Ocean, the verification was previously done by testing the robustness of the constraint to changes in the definition of the inter-frontal zone (Terhaar et al., 2021b). Further evidence for the underlying mechanism was provided by a later study that analysed explicitly the stratification in the water column (Bourgeois et al., 2022). Similarly, it was shown that the transport of C_{ant} by the AMOC is crucial for the C_{ant} uptake in the North Atlantic (Buckley and Marshall, 2016; Goris et al., 2018). As the AMOC is predominantly observed at 26.5°N, a change to the definition is not possible. Instead, we replaced the AMOC as a predictor by another indicator for deep-water formation, namely the area of waters in the North Atlantic below which the water column is weakly stratified (see Appendix A.1 and Table A.1.4) (Hess, 2022). The results remain almost unchanged, indicating the robustness of the constraint and that the AMOC is indeed a good indicator for the stability of the water column in the North Atlantic and the associated deep-water formation. To provide further indication for the importance of the AMOC and the Southern Ocean surface salinity, we have compared simulated CFC-11, provided by 10 ESMs from CMIP6, with observed CFC-11 from GLODAPv2.2021 (Lauvset et al., 2021) (Appendix A.3). The comparison demonstrates the importance of the AMOC for the ventilation of the North Atlantic, as ESMs with a low AMOC underestimate the observed subsurface CFC-11 concentrations in the North Atlantic. Similarly, ESMs with a small inter-frontal Southern Ocean surface salinity underestimate observed subsurface (below 200 m) CFC-11 concentrations in the Southern hemisphere. Eventually, we have also tested the robustness of the biogeochemical predictor, by varying the definition of the Revelle factor. First, the Revelle factor was only calculated north of 45°N and south of 45°S, assuming that the high-latitude regions are responsible for the largest C_{ant} uptake, and second, the global Revelle factor was calculating by weighting the Revelle factor in each cell by the multi-model mean cumulative C_{ant} uptake from 1850 to 2100 in that cell so that the Revelle factor in cells with larger uptake is more strongly weighted. Under both definitions, the results remain almost unchanged (Table A.1.4), suggesting that the globally averaged Revelle factor is a robust predictor of ocean C_{ant} uptake.

To validate the here identified constraint in another model ensemble, we used all six ESMs of the CMIP5 ensemble that provided all necessary output variables (Table A.1.1). As these six ESMs are not sufficient to robustly fit a function with four

https://doi.org/10.5194/bg-2022-134
Preprint. Discussion started: 20 June 2022

unknown parameters, we applied the predicted relationship by the CMIP6 models to the CMIP5 models and evaluated how well this relationship allows to predict the simulated historical C_{ant} uptake by these models. The CMIP6 derived relationship allows to predict the simulated C_{ant} uptake with an accuracy of 3% (±5 Pg C) for the period from 1850 to 2014 and with an accuracy of 4% (±1.3 Pg C) for the period from 1994 to 2007 (Figure A.4.1). The largest uncertainty stems from the NorESM2-ME model, which simulates a historical AMOC strength of ~30 Sv, almost twice as large as the observed AMOC strength and ~9 Sv larger than all other CMIP6 ESMs over which the relationship was fitted. For such strong deviations from the observations and other ESMs, the linear relationship might not be applicable anymore. However, despite one out of six ESMs from CMIP5 having a particularly high AMOC, the here identified relationship still allows to predict the simulated C_{ant} uptake with small uncertainties and hence confirms its applicability.

Despite this robustness, emergent constraints are, by definition, always relying on the existing ESMs and on the processes that are represented by these ESMs. If certain processes are not implemented or implemented in the same way across all ESMs, biases over the entire model ensemble can occur that cannot be corrected by an emergent constraint (Sanderson et al., 2021). Possible non-represented processes in our case are among others changing freshwater input from the Greenland and Antarctic ice sheet that may impact the freshwater cycle and circulation in the Southern Ocean or the AMOC, and changes in riverine input of carbon over time. However, the expected effect of ice melt on sea surface salinity in the Southern Ocean and on the AMOC is small compared to the model spread (Bakker et al., 2016; Terhaar et al., 2021b), at least on the timescales considered here. Changing riverine carbon fluxes could, however, have a larger effect. So far, only one CMIP6 ESM, the CNRM-ESM2-1 (Séférian et al., 2019), has dynamic carbon riverine delivery that changes with global warming. In this model, carbon riverine delivery increases over the 20st century so that the interior ocean change in C_{ant} in 2000 is around 19 Pg C smaller than the air-sea C_{ant} uptake (Figure A.1.3). The situation reverses at the beginning of the 21st century, so that riverine carbon delivery increases and the interior ocean change in C_{ant} becomes up to 60 Pg C larger than the air-sea C_{ant} uptake. As such, riverine carbon delivery has the potential to enhance or decrease the ocean C_{ant} inventory in addition to air-sea C_{ant} uptake. This would also question the comparability of C_{ant} inventory and air-sea C_{ant} uptake estimates. However, the present state of the ESMs does not allow a quantitative assessment of this process and future research is needed.

https://doi.org/10.5194/bg-2022-134
Preprint. Discussion started: 20 June 2022

6 Conclusion

The here identified three-dimensional emergent constraint allows identifying a bias towards too low C_{ant} uptake by ESMs from CMIP6, reduced uncertainties of the global ocean C_{ant} sink, and led to an enhanced process understanding of the C_{ant} uptake in ESMs. The constraint was tested for robustness in multiple ways and across different model ensembles. The constraint demonstrates that the global ocean C_{ant} uptake can be estimated from three observable variables, the salinity in the subtropical-polar frontal zone in the Southern Ocean, the Atlantic Meridional Overturning Circulation, and the global surface ocean Revelle factor. Improved or continuing observations of these quantities (Lauvset et al., 2016; Zweng et al., 2018; Locarnini et al., 2018; Claustre et al., 2020; McCarthy et al., 2020) and their representation and evaluation in ESMs and ocean models should therefore be of great priority in the next years and decades. Biases in these quantities and corrections for the late starting date may well be the reason for mismatches between models and observations (Hauck et al., 2020; Friedlingstein et al., 2022; Crisp et al., 2022) and should be evaluated when analysing and presenting simulated ocean C_{ant} uptake.

The larger than previously estimated future ocean C_{ant} sink corresponds to around 2 to 4 years of present-day CO_2 emissions (~10.5 Pg C yr^{-1}) depending on the emissions pathway. The larger ocean C_{ant} sink thus increases the estimated remaining emission budget, but only by a small amount. However, it also results in enhanced projected ocean acidification that may be harmful for large, unique ocean ecosystems (Fabry et al., 2008; Gruber et al., 2012; Kawaguchi et al., 2013; Kroeker et al., 2013; Doney et al., 2020; Hauri et al., 2021; Terhaar et al., 2021a).

This study follows recent approaches by the IPCC and climate science that suggest using the best available information about models instead of a multi-model mean to provide consistent and accurate information for climate science and policy (IPCC, 2021; Hausfather et al., 2022). The here provided improved estimate of the size of the global ocean carbon sink may help to close the carbon budget imbalance (Friedlingstein et al., 2022) and to improve the understanding of the overall carbon cycle and the global climate (IPCC, 2021). Eventually, a better understanding of the ocean carbon sink and the reduction of its uncertainties in the past and in the future allows better targeted climate and ocean policies (IPCC, 2022).

https://doi.org/10.5194/bg-2022-134
Preprint. Discussion started: 20 June 2022

Biogeosciences Discussions Open Access EGU

Appendix A

A.1 Earth System Models

Model output from 18 Earth System Models from CMIP6 and 6 Earth System Models from CMIP5 (Table A.1.1) were used for the analyses.

370

Table A.1.1 CMIP5 and CMIP6 models used in this study and the corresponding model groups

Model name*	Modeling center	References
ACCESS-ESM1-5	Commonwealth Scientific and Industrial Research Organisation (CSIRO)	(Ziehn et al., 2020)
CanESM2		
CanESM5	Canadian Centre for Climate Modelling and Analysis	(Chylek et al., 2011; Christian et al., 2022)
CanESM5-CanOE		
CESM1-BGC		
CESM2	Community Earth System Model Contributors	(Gent et al., 2011; Lindsay et al., 2014; Danabasoglu et al., 2020)
CESM2-WACCM		
CMCC-ESM2	Centro Euro-Mediterraneo per I Cambiamenti Climatici	(Lovato et al., 2022)
CNRM-ESM2-1	Centre National de Recherches Meteorologiques / Centre Europeen de Recherche et Formation Avancees en Calcul Scientifique	(Séférian et al., 2019)
EC-Earth3-CC	EC-Earth consortium (http://www.ec-earth.org/community/consortium/)	(Döscher et al., 2022)
GFDL-ESM2M		
GFDL-CM4	NOAA Geophysical Fluid Dynamics Laboratory (NOAA GFDL)	(Dunne et al., 2012; Held et al., 2019; Dunne et al., 2020; Stock et al., 2020)
GFDL-ESM4		
IPSL-CM6A-LR	Institut Pierre-Simon Laplace (IPSL)	(Boucher et al., 2020)
MIROC-ES2L	Japan Agency for Marine-Earth Science and Technology, Atmosphere and Ocean Research Institute (The University of Tokyo), and National Institute for Environmental Studies	(Hajima et al., 2020)
MPI-ESM-LR		
MPI-ESM-MR	Max-Planck-Institut für Meteorologie (Max Planck Institute for Meteorology)	(Giorgetta et al., 2013; Mauritsen et al., 2019; Gutjahr et al., 2019)
MPI-ESM-1-2-LR		
MPI-ESM-1-2-HR		
MRI-ESM2-0	Meteorological Research Institute (Japan Meteorological Agency)	(Yukimoto et al., 2019)
NorESM1-ME		
NorESM2-LM	Norwegian Climate Centre	(Bentsen et al., 2013; Tjiputra et al., 2020)
NorESM2-MM		
UKESM1-0-LL	Met Office Hadley Centre	(Sellar et al., 2020)

*CMIP5 models are written in italics

https://doi.org/10.5194/bg-2022-134
Preprint. Discussion started: 20 June 2022

The analysed variables include the air-sea CO_2 flux (fgco2, name of the variable in standardized CMIP output), total dissolved inorganic carbon (dissic), total alkalinity (talk), total dissolved inorganic silicon (si), total dissolved inorganic phosphorus (po4), potential temperature (thetao), salinity (so), and the Atlantic meriodional streamfunction (msftmz or msftyz). All ESMs were included for which the entire set of variables was available on the website of the Earth System Grid Federation at the start of the analysis. Based on these variables, all other presented variables were derived:

- The air-sea C_{ant} flux was calculated as the difference in air-sea CO_2 flux between the historical plus future (SSP for CMIP6 and RCP for CMIP5) simulation and the correspondent pre-industrial control simulation on the native model grids (where possible). The air-sea C_{ant} fluxes were corrected for their late starting date in 1850 (and 1861 for GFDL-ESM2M) and the slightly higher atmospheric CO_2 mixing ratio in that year compared to the beginning of the industrialization and the start of the CO_2 increase in 1765 (Bronselaer et al., 2017). To that end, we scaled the simulated air-sea C_{ant} flux with the anthropogenic change in the atmospheric partial pressure of CO_2 (pCO_2) with respect to pre-industrial conditions following previous studies (Mikaloff Fletcher et al., 2006; Gruber et al., 2009; Terhaar et al., 2021b):

$$C_{ant}^{corr}(t) = C_{ant}(t)\frac{pCO_2(t)-pCO_2(1765)}{pCO_2(t)-pCO_2(1850)}, \quad (1)$$

with $C_{ant}(t)$ being the simulated air-sea C_{ant} flux by the respective ESM in year t and $C_{ant}^{corr}(t)$ being the corrected air-sea C_{ant} flux. For GFDL-ESM2M, which starts in 1861, the correction was made with respect to $pCO_2(1861)$. When $pCO_2(t)$ is close to $pCO_2(1850)$, their difference becomes unrealistically large, causing overly strong flux corrections. Therefore, we limited the flux correction in magnitude using the correction term in year 1950 as an upper limit. By doing so, we do not only remove unrealistically high air-sea C_{ant} fluxes before 1950 but also reach excellent agreement with the previously estimated air-sea C_{ant} fluxes correction term by Bronselaer et al. (2017) (Figure A.1.1). When the cumulative C_{ant} fluxes since 1765 are shown, an additional amount of 12 Pg C (16 Pg C for GFDL-ESM2M) was added that was estimated to have entered the ocean before 1850 (Bronselaer et al., 2017). For comparison, we

https://doi.org/10.5194/bg-2022-134
Preprint. Discussion started: 20 June 2022

also calculated the constrained estimates for the ocean C_{ant} sink when no air-sea C_{ant} flux correction is applied (Table A.1.2). Bronselaer et al. (2017) estimate the uncertainty of the correction to be ±16% for cumulative C_{ant} fluxes from 1765 to 1995. Although uncertainties reduce over time, we apply the 16% from the past to all estimates and hence provide a conservative upper bound of this uncertainty.

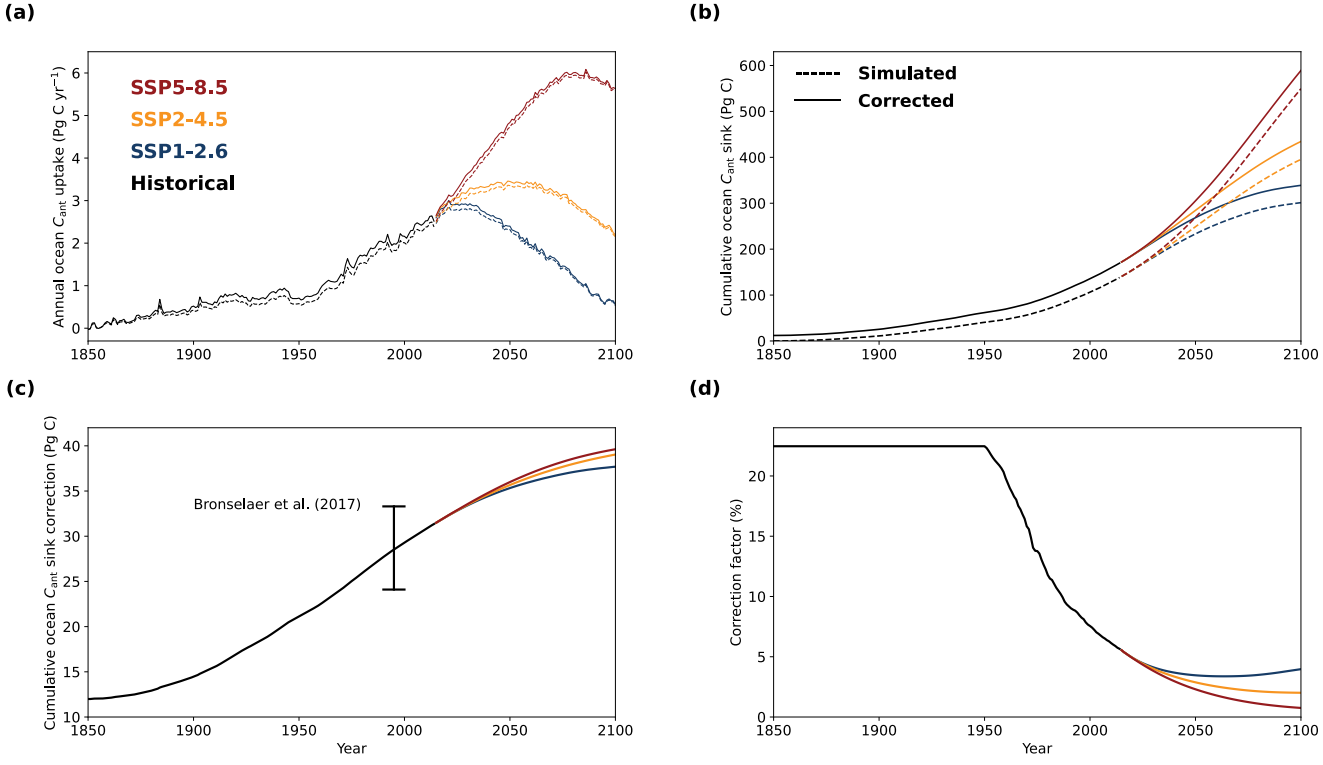

Figure A.1.1. Correction of simulated anthropogenic carbon air-sea flux for the late starting date in Earth System Models. Multi-model **a)** annual mean anthropogenic carbon (C_{ant}) air-sea flux for 17 ESMs from CMIP6 before (dashed lines) and after (solid lines) the correction for the late starting date over the historical period from 1850 to 2014 (black) and for the future from 2015 to 2100 under SSP1-2.6 (blue), SSP2-4.5 (orange), and SSP5-8.5 (red). **b)** Cumulative ocean C_{ant} uptake since 1765 (corrected simulated flux) and 1850 (raw simulated flux), **c)** difference between cumulative ocean C_{ant} uptake between corrected and raw simulated flux, and **d)** the correction factor that was applied. The C_{ant} correction that was estimated by Bronselaer et al. (2017) is shown for in **c)**. The cumulative C_{ant} uptake from 1765 to 1850 was set to 12 Pg C as estimated by Bronselaer et al. (2017).

https://doi.org/10.5194/bg-2022-134
Preprint. Discussion started: 20 June 2022

Table A.1.2. Global ocean air-sea CO_2 flux estimates based on 17 ESMs from CMIP6 before and after constraint over different periods with corrected and uncorrected estimates and with and without CNRM-ESM2-1. Prior uncertainty is the multi-model standard deviation and constrained uncertainty is a combination of the multi-model standard deviation after correction and the uncertainty from the correction itself (see Appendix A.3).

Period	Cumulative air-sea C_{ant} flux (Pg C)					
	Raw simulated		Starting date corrected		Corrected + CNRM-ESM2-1	
	Prior	Constrained	Prior	Constrained	Prior	Constrained
1994-2007	26.8 ± 2.1	29.3 ± 0.8	28.8 ± 2.2	31.5 ± 0.9	28.6 ± 2.3	31.3 ± 1.2
1850-2014	138 ± 10	150 ± 5	157 ± 12	171 ± 5	156 ± 12	171 ± 6
1850-2020	154 ± 11	167 ± 5	174 ± 13	189 ± 6	173 ± 13	189 ± 6
2020-2100 (SSP1-2.6)	150 ± 11	167 ± 7	156 ± 11	173 ± 7	156 ± 11	173 ± 7
2020-2100 (SSP2-4.5)	244 ± 16	269 ± 8	251 ± 17	277 ± 9	251 ± 16	276 ± 9
2020-2100 (SSP5-8.5)	399 ± 29	436 ± 11	407 ± 30	445 ± 11	405 ± 29	444 ± 12

- Accordingly, the change in ocean interior C_{ant} was calculated as the difference in total dissolved inorganic carbon between the historical plus future (SSP/RCP) simulation and the correspondent pre-industrial control simulation on the native model grids (where possible).
- The change in air-sea CO_2 flux that is caused by a changing climate was calculated as the difference in fgco2 in the historical simulation and the 'bgc' simulation in which only atmospheric CO_2 changes, but not the climate. These 'bgc' simulations were available for 5 ESMs (Table A.1.3)

https://doi.org/10.5194/bg-2022-134
Preprint. Discussion started: 20 June 2022


Biogeosciences Discussions Open Access EGU

Table A.1.3. Climate-driven changes in the air-sea CO_2 flux (Pg C yr^{-1}) as simulated by 5 Earth System Models from CMIP6

Year	Climate-driven changes in the cumulative air-sea CO_2 flux (Pg C)						
	ACCESS-ESM1-5	CanESM5	MIROC-ES2L	MRI-ESM2-0	NorESM2-LM	Multi-model mean	Multi-model standard deviation
1994-2007	-1.7	-1.7	-1.4	-2.2	-0.7	-1.6	0.5

.

- The surface ocean Revelle factor was calculated from sea surface total dissolved inorganic carbon (dissic), total alkalinity (talk), total dissolved inorganic silicon (si), total dissolved inorganic phosphorus (po4), potential temperature (thetao), and salinity (so) averaged around the year 2002 (from 1997 to 2007 for CMIP6 and 1999 to 2005 for CMIP5; 2005 is the last year of the historical simulation) using *mocsy2.0* (Orr and Epitalon, 2015) with its default constants that are recommended for best practice (Dickson et al., 2007). The years were centred around 2002 to make the Revelle factor comparable to the one estimated based on GLODAPv2, which is normalized to the year 2002 (Lauvset et al., 2016). As the Revelle factor describes the relative change in C_T per relative change in pCO_2 (Revelle and Suess, 1957), the absolute uptake of C_T does not only depend on the Revelle factor but also on the natural C_T in the surface ocean. To calculate the buffer capacity for each ESM, the Revelle factor was therefore adjusted in each grid cell by multiplying it by the ratio of observed C_T and the simulated C_T in each ESM separately. Data from each ESM was regridded on a regular 1°x1° grid to make it comparable to the gridded GLODAPv2 data. Furthermore, a mask was applied before the basin-wide averaged Revelle factor was calculated so that only values were used where all ESMs and the gridded GLODAPv2 product had data. In addition, marginal seas (Mediterranean Sea, Hudson Bay, Baltic Sea) were excluded because global ESMs are not designed to accurately represent these small-scale seas. In addition, the surface ocean carbonate ion (CO_3^{2-}) concentration was calculated that the C_T-adjusted Revelle factor is mainly determined by the CO_3^{2-} concentrations, which itself can be approximated by the difference between surface ocean alkalinity and C_T (Figure A.1.2).

https://doi.org/10.5194/bg-2022-134
Preprint. Discussion started: 20 June 2022

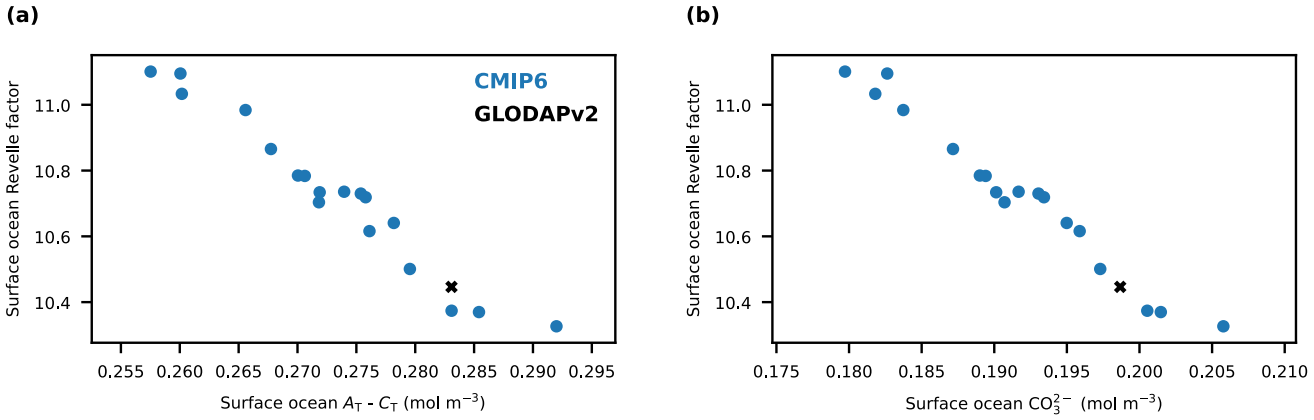

Figure A.1.2. Surface ocean Revelle factor against the difference of surface alkalinity and dissolved inorganic carbon, and against surface carbonate ion concentrations. Basin-wide averaged surface ocean Revelle factor as simulated by 18 ESMs from CMIP6 (blue dots) against the basin-wide averaged surface ocean **a)** total dissolved inorganic carbon (C_T), **b)** total alkalinity (A_T), **c)** their difference (A_T - C_T), and **d)** carbonate ion (CO_3^{2-}) concentrations. The observation-based estimates from GLODAPv2 are shown as black crosses. The Revelle factor in each ESM was adjusted for biases in the surface ocean C_T (see Appendix A.1).

- The monthly AMOC strength was calculated as the maximum of the streamfunction below 500 m at the latitude in the respective model that is closest to 26.5°N for each month from 2004 to 2020. After 2014, simulated output from SSP5-8.5 and RCP4.5 were used as all ESMs provided output for these pathways. For SSP5-8.5, the mole fraction of atmospheric CO_2 in SSP5-8.5 is 414.9 ppm in 2020 (Meinshausen et al., 2020), 2.5 ppm over the observed mole fraction of atmospheric CO_2 in 2020 (Trends in Atmospheric Carbon Dioxide (NOAA/GML)). For RCP4.5, the mole fraction of atmospheric CO_2 is 412.4 ppm in 2020. Such small differences in the mole fraction of atmospheric CO_2 do not cause detectable changes in global warming or the AMOC (IPCC, 2021).
- Future saturation states of aragonite were calculated from simulated changes in total dissolved inorganic carbon (dissic), total alkalinity (talk), total dissolved inorganic silicon (si), total dissolved inorganic phosphorus (po4), potential temperature (thetao) and salinity (so) since 2002 that are added to the respective observed variables from the gridded GLODAPv2 product, which are normalized to 2002, using *mocsy2.0* (Orr and Epitalon, 2015) with its default constants that are recommended for best practice (Dickson et al., 2007). By only adding simulated difference,

https://doi.org/10.5194/bg-2022-134
Preprint. Discussion started: 20 June 2022

model uncertainties in the initial state of the ocean biogeochemical system in the deeper ocean are removed (Orr et al., 2005; Terhaar et al., 2020a, 2021a, b). All variables were regridded before on a regular 1°x1° grid so that they could be added to the gridded GLODAPv2 data. The same mask that was also used to compare the Revelle factor was applied to make all projections comparable.

- The annual average sea surface salinity between the polar and subtropical front in the Southern Ocean was derived from regridded (1°x1° regular grid) monthly sea surface salinity and temperatures (for defining the fronts) following (Terhaar et al., 2021b).
- The area of weakly stratified waters was calculated based on climatologies of the potential temperature and salinity from 1995 to 2014 (Hess, 2022). All data was regridded on a regular 1°x1° grid with 33 depth levels before analysis. An area was defined as weakly stratified if the density gradient between the surface and the cell at 1000 m depth was smaller than 0.5 kg m^{-3} in a given month, assuming that such a small monthly mean gradient allows mixing of water into the lower limb of the AMOC at some time in that month. This predictor, as well as the different ways of calculating the Revelle factor predictor (see section "Robustness of the emergent constraint and possible impact of changing riverine carbon input over time"), was used to test the robustness of the here identified emergent constraint (Table A.1.4).

The model CNRM-ESM2-1 was not used for the constraints because it includes dynamical riverine forcing that no other model includes (Figure A.1.3) and is not directly comparable. Instead, output from this ESM was prominently used in the section "Robustness of the emergent constraint and possible impact of changing riverine carbon input over time". However, even if CNRM-ESM2-1 had been included, the results change by less than 1% (Table A.1.2).

https://doi.org/10.5194/bg-2022-134
Preprint. Discussion started: 20 June 2022

Table A.1.4. Constrained global ocean air-sea CO_2 flux estimates based on 17 ESMs from CMIP6 with varying predictors.

Period	Cumulative air-sea C_{ant} flux (Pg C)			
	Standard	Revelle factor		Area of weakly stratified water column
		>45°N & <45°S	Flux-weighted	
1994-2007	31.5 ± 0.9 (r^2=0.87)	31.6 ± 1.1 (r^2=0.80)	31.7 ± 1.0 (r^2=0.83)	31.3 ± 1.1 (r^2=0.78)
1850-2014	171 ± 6 (r^2=0.80)	172 ± 8 (r^2=0.65)	173 ± 7 (r^2=0.73)	171 ± 7 (r^2=0.74)
1850-2020	189 ± 7 (r^2=0.80)	190 ± 8 (r^2=0.64)	191 ± 8 (r^2=0.72)	189 ± 7 (r^2=0.73)
2020-2100 (SSP1-2.6)	173 ± 8 (r^2=0.56)	173 ± 8 (r^2=0.56)	172 ± 8 (r^2=0.55)	171 ± 8 (r^2=0.53)
2020-2100 (SSP2-4.5)	277 ± 9 (r^2=0.74)	278 ± 9 (r^2=0.71)	277 ± 9 (r^2=0.71)	274 ± 9 (r^2=0.72)
2020-2100 (SSP5-8.5)	445 ± 12 (r^2=0.87)	450 ± 13 (r^2=0.83)	449 ± 12 (r^2=0.84)	442 ± 12 (r^2=0.84)

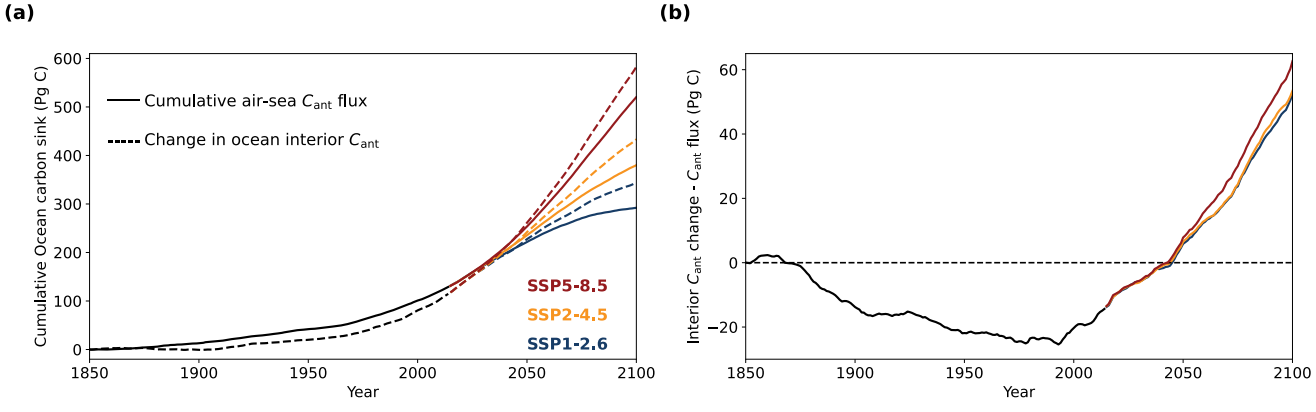

Figure A.1.3. Anthropogenic carbon air-sea fluxes and inventory changes simulated by CNRM-ESM2-1. **(a)** Cumulative air-sea anthropogenic carbon (C_{ant}) fluxes (solid lines) and C_{ant} interior changes (dashed lines) as simulated by CNRM-ESM2-1 for the historic period until 2014 (black) and from 2015 to 2100 under SSP1-2.6 (blue), SSP2-4.5 (orange), and SSP5-8.5 (red), **(b)** as well as the difference of both quantities. The thin dashed black line in **(b)** indicates zero difference.

https://doi.org/10.5194/bg-2022-134
Preprint. Discussion started: 20 June 2022

A.2 Observations and observation-based products

Throughout this manuscript, three observation-based products are used to constrain the ESM output:

- Monthly climatologies of sea surface salinity and sea surface temperatures from the World Ocean Atlas 2018 (Zweng et al., 2018; Locarnini et al., 2018) were used to derive annual averages and uncertainties of the sea surface salinity between the polar and subtropical fronts in the Southern Ocean following Terhaar et al. (2021b). Climatologies of the World Ocean Atlas 2018 were also used to calculate the area of weakly stratified surface waters.
- Time series of the AMOC strength from the RAPID array (McCarthy et al., 2020) were used to calculate monthly means and uncertainties of the AMOC from 2004 to 2020.
- The gridded observation-based estimates of total dissolved inorganic carbon, total alkalinity, total dissolved inorganic silicon, total dissolved inorganic phosphorus, in-situ temperature, and salinity from GLODAPv2 (Lauvset et al., 2016) were used to calculate the Revelle factor and as a starting point for projected saturation states over the 21st century (see above).

A.3 Applying the constraint and uncertainty estimation

For the three-dimensional emergent constraint, multi-linear regression was used. First, it was assumed that the ocean C_{ant} uptake for every model M (C_{ant}^{M}) can be approximated by a linear combination of the inter-frontal sea surface salinity in the Southern Ocean in model M ($SSS_{Southern\ Ocean}^{M}$), the AMOC strength in model M ($AMOC^{M}$), and the globally-averaged surface ocean Revelle factor in model M ($Revelle_{global}^{M}$):

$$C_{ant}^{M} = a * SSS_{Southern\ Ocean}^{M} + b * AMOC^{M} + c * Revelle_{global}^{M} + d + \varepsilon. \quad (2)$$

The parameters a, b, and c are scaling parameters of the three predictor variables, d is the y intercept, and ε describes the residual between the predicted C_{ant} flux by this multi-linear regression model and the simulated C_{ant} uptake by model M. The free parameters a, b, c, and d were fitted based on the simulated inter-frontal sea surface salinity in the Southern Ocean, AMOC, Revelle factor, and C_{ant} uptake.

https://doi.org/10.5194/bg-2022-134
Preprint. Discussion started: 20 June 2022

520

Afterwards the constrained C_{ant} flux is estimated by replacing the simulated inter-frontal sea surface salinity in the Southern Ocean, AMOC, and Revelle factor by the observed ones and by setting ε to zero. As the Revelle factor describes the inverse of the ocean capacity to take up C_{ant} from the atmosphere, equation (2) should in principal be used with $\frac{1}{Revelle^{M}_{global}}$. However, using $Revelle^{M}_{global}$ facilitates understanding and the presentation of the results and only introduces maximum errors of around 0.1% for the Revelle factor adjustment for the models that simulate the largest deviations from the observed Revelle factor. To estimate the uncertainty, all model results were first corrected for their biases in the three predictor variables, i.e., if a model has a salinity that is 0.2 smaller than the observed salinity, the simulated C_{ant} uptake by this model is increased by $a * 0.2$. The same correction is made for the other two predictor variables (Figure 3). If the three predictor variables were predicting the C_{ant} flux perfectly, the bias-corrected C_{ant} uptake from all models would be the same. The remaining inter-model standard deviation therefore represents the uncertainty from the multi-linear regression model due to other factors that influence the ocean C_{ant} uptake. The second part of the uncertainty originates from the uncertainty in the observations of the predictor variables that influences the magnitude of the correction. This uncertainty (ΔC^{obs}_{ant}) is calculated as follows:

525

530

$$\Delta C^{obs}_{ant} = \sqrt{(a * \Delta SSS^{obs}_{Southern\ Ocean})^2 + (b * \Delta AMOC^{obs})^2 + \left(c * \Delta Revelle^{obs}_{global}\right)^2}, \quad (3)$$

535

with $\Delta SSS^{obs}_{Southern\ Ocean}$, $\Delta AMOC^{obs}$, and $\Delta Revelle^{obs}_{global}$ being the uncertainty of the three observed predictor variables. Eventually, the overall uncertainty of this constrained C_{ant} flux is estimated as the square-root of the sum of the product of the square of both uncertainties.

540

A.4 Validation of the identified constraint in CMIP5

The here identified emergent constraint was derived from an ensemble of 17 ESMs from CMIP6. To test the robustness of emergent constraints, these constraints should be validated in an independent ensemble of ESMs (Hall et al., 2019). Here, we used all 6 ESMs from CMIP5 that provided all necessary output variables for this analysis (see Appendix A.1). For all these

https://doi.org/10.5194/bg-2022-134
Preprint. Discussion started: 20 June 2022

models, the C_{ant} uptake for the period from 1994 to 2007 and from 1850 to 2014 was predicted based on the simulated inter-frontal sea surface salinity in the Southern Ocean, the AMOC strength, and the global ocean basin-wide averaged Revelle factor using the multi-linear relationship derived from the CMIP6 models (Figure A.4.1).

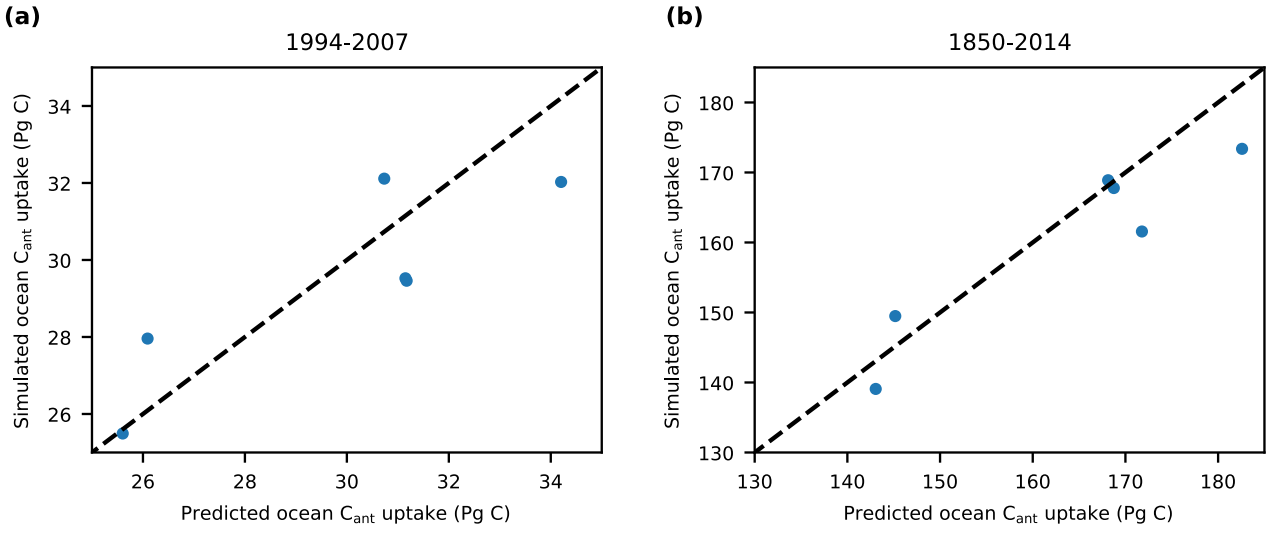

Figure A.4.1. Global ocean anthropogenic carbon uptake simulated by Earth System Models from CMIP5 against the predicted uptake based on simulated predictors from CMIP6 models. Global ocean anthropogenic carbon uptake simulated by 6 ESMs from CMIP5 (Table A.1.1) **a)** from 1994 to 2007 and **b)** from 1850 to 2014 against the predicted anthropogenic carbon uptake based on the simulated CMIP6 predictors in each ESM: the inter-frontal annual mean sea surface salinity in the Southern Ocean, the Atlantic Meridional Overturning Circulation, and the Revelle factor adjusted for surface ocean C_T. Please note that two ESMs are at almost the same place in **a)** with a predicted C_{ant} uptake of around 31 Pg C.

A.5 Comparison between simulated and observed CFC-11 concentrations

Comparison between simulated and observed CFC-11 uptake allows to estimate the ventilation of waters from the surface waters to the deeper ocean (Hall et al., 2002). Although CFCs can roughly evaluate the ventilation rate of the ocean, no perfect agreement between CFCs and C_{ant} can be expected as CFCs are not taken up at the same speed as C_{ant} (i.e., fast air-sea equilibration time scale for CFC) and their solubility has a different temperature dependency than the solubility of C_{ant} (warm waters can hold less CFCs but more C_{ant} due to their low Revelle factor, whereas cold waters hold more CFCs but less C_{ant}) (Revelle and Suess, 1957; Broecker and Peng, 1974; Weiss, 1974). These differences can lead to differences between uptake,

https://doi.org/10.5194/bg-2022-134
Preprint. Discussion started: 20 June 2022

storage, and distribution of CFCs and C_{ant} that can become especially large in high-latitude oceans (Matear et al., 2003; Terhaar et al., 2020b).

565

Here, we use simulated CFC-11 from ESMs and observed CFC-11 from GLODAPv2.2021 (Lauvset et al., 2021) to provide further evidence that the inter-frontal sea surface salinity in the Southern Ocean and the AMOC are good indicators for the ocean ventilation and that ESMs tend to underestimate the ventilation of surface waters to the deeper ocean. Out of the 18 ESMs from CMIP6, 10 provided simulated 3D-fields of CFC-11 (CanESM5, CESM2, CESM2-WACCM, EC-Earth-CC,
570 GFDL-CM4, GFDL-ESM4, MRI-ESM2-0, NorESM2-LM, NorESM2-MM, UKESM1-0-LL). To compare these ESMs to the observed concentrations, all ESMs were sampled at the same time (month and year), the same latitude and longitude, and the same depth as the observations. To assess the ventilation below the mixed layer, we only used observations below 200 m. Furthermore, we limited our assessment to observations until 2004 as CFC-11 in the atmosphere has peaked in 1994 (Bullister, n.d.) and subducted waters since then might already re-emerge to the surface. Thus, 506000 measurements remained. As these
575 measurements are not equally distributed, and strongly clustered in the Northern hemisphere (Lauvset et al., 2021), we mapped all measurements on a regular 5°x5° grid with 11 depth levels from 200 m to 6000 m that increase with depth. In each cell on the grid the average bias was calculated. Afterwards, the volume averaged bias was calculated for the Southern hemisphere and the North Atlantic (limited by the equator and 65°N) (Figure A.5.1).

580

https://doi.org/10.5194/bg-2022-134
Preprint. Discussion started: 20 June 2022

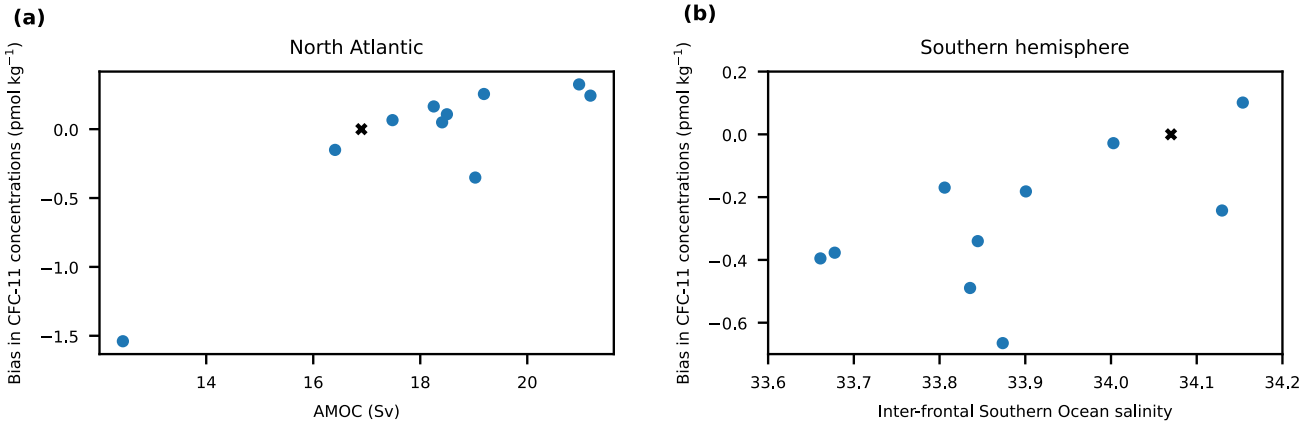

Figure A.5.1. Biases in subsurface CFC-11 concentrations between observations against the Atlantic Meridional Overturning circulation and the Inter-frontal Southern Ocean Salinity. Basin-wide averaged biases in CFC-11 concentrations (observations minus simulated) below 200 m for all 10 ESMs that provided simulated CFC-11 (blue dots) **(a)** in the North Atlantic Ocean (north of the equator and limited by the Fram Strait, the Barents Sea Opening, and the Baffin Bay) and against the AMOC and **(b)** in the Southern hemisphere (south of the equator) against the inter-frontal annual mean sea surface salinity in the Southern Ocean. The observation-based estimates for the AMOC and the inter-frontal annual mean sea surface salinity in the Southern Ocean are shown as black crosses and with zero bias in CFC-11.

https://doi.org/10.5194/bg-2022-134
Preprint. Discussion started: 20 June 2022

Code availability

The mocsy2.0 code is publicly available via https://github.com/jamesorr/mocsy.

Data availability

All model output from CMIP is available via https://esgf-node.llnl.gov/search/cmip6/.

Author Contributions

Conceptualization: JT

Methodology: JT

Software: JT

Investigation: JT

Visualization: JT

Funding acquisition: TLF, FJ

Project administration: TLF, FJ

Writing – original draft: JT

Writing – review & editing: JT, TLF, FJ

Competing interests

Authors declare that they have no conflict of interests.

Acknowledgements

This work was funded by the European Union's Horizon 2020 research and innovation programme under grant agreement No 821003 (project 4C, Climate-Carbon Interactions in the Current Century) (JT, TLF,FJ) and No 820989 (project COMFORT, Our common future ocean in the Earth system-quantifying coupled cycles of carbon, oxygen and nutrients for determining and achieving safe operating spaces with respect to tipping points) (TLF,FJ), and by the Swiss National Science Foundation under

https://doi.org/10.5194/bg-2022-134
Preprint. Discussion started: 20 June 2022

grant PP00P2_198897 (TLF) and grant #200020_200511 (JT, FJ). The work reflects only the authors' view; the European Commission and their executive agency are not responsible for any use that may be made of the information the work contains. We also thank Donat Hess for his work on the North Atlantic anthropogenic carbon uptake during his master thesis at our institute, as well as Friedrich Burger, Nadine Goris and Jens Müller for discussions.

https://doi.org/10.5194/bg-2022-134
Preprint. Discussion started: 20 June 2022

References

630 Albright, R., Caldeira, L., Hosfelt, J., Kwiatkowski, L., Maclaren, J. K., Mason, B. M., Nebuchina, Y., Ninokawa, A., Pongratz, J., Ricke, K. L., Rivlin, T., Schneider, K., Sesboüé, M., Shamberger, K., Silverman, J., Wolfe, K., Zhu, K., and Caldeira, K.: Reversal of ocean acidification enhances net coral reef calcification, Nature, 531, 362–365, https://doi.org/10.1038/nature17155, 2016.

635 Aumont, O., Orr, J. C., Monfray, P., Ludwig, W., Amiotte-Suchet, P., and Probst, J.-L.: Riverine-driven interhemispheric transport of carbon, Global Biogeochem. Cycles, 15, 393–405, https://doi.org/https://doi.org/10.1029/1999GB001238, 2001.

Bakker, P., Schmittner, A., Lenaerts, J. T. M., Abe-Ouchi, A., Bi, D., van den Broeke, M. R., Chan, W.-L., Hu, A., Beadling, R. L., Marsland, S. J., Mernild, S. H., Saenko, O. A., Swingedouw, D., Sullivan, A., and Yin, J.: Fate of the Atlantic Meridional Overturning Circulation: Strong decline under continued warming and Greenland melting, Geophys. Res. Lett., 43, 12,212-

640 252,260, https://doi.org/https://doi.org/10.1002/2016GL070457, 2016.

Bednaršek, N., Tarling, G. A., Bakker, D. C. E., Fielding, S., and Feely, R. A.: Dissolution Dominating Calcification Process in Polar Pteropods Close to the Point of Aragonite Undersaturation, PLoS One, 9, https://doi.org/10.1371/journal.pone.0109183, 2014.

645

Behrenfeld, M. J., Gaube, P., Della Penna, A., O'Malley, R. T., Burt, W. J., Hu, Y., Bontempi, P. S., Steinberg, D. K., Boss, E. S., Siegel, D. A., Hostetler, C. A., Tortell, P. D., and Doney, S. C.: Global satellite-observed daily vertical migrations of ocean animals, Nature, 576, 257–261, https://doi.org/10.1038/s41586-019-1796-9, 2019.

650 Bendtsen, J., Lundsgaard, C., Middelboe, M., and Archer, D.: Influence of bacterial uptake on deep-ocean dissolved organic carbon, Global Biogeochem. Cycles, 16, 74-1-74–12, https://doi.org/https://doi.org/10.1029/2002GB001947, 2002.

Bennington, V., Gloege, L., and McKinley, G. A.: Observation-based variability in the global ocean carbon sink from 1959-2020, Earth Sp. Sci. Open Arch., 14, https://doi.org/10.1002/essoar.10510815.1, 2022.

655

Bentsen, M., Bethke, I., Debernard, J. B., Iversen, T., Kirkevåg, A., Seland, Ø., Drange, H., Roelandt, C., Seierstad, I. A., Hoose, C., and Kristjánsson, J. E.: The Norwegian Earth System Model, NorESM1-M – Part 1: Description and basic evaluation of the physical climate, Geosci. Model Dev., 6, 687–720, https://doi.org/10.5194/gmd-6-687-2013, 2013.

660 Boucher, O., Servonnat, J., Albright, A. L., Aumont, O., Balkanski, Y., Bastrikov, V., Bekki, S., Bonnet, R., Bony, S., Bopp, L., Braconnot, P., Brockmann, P., Cadule, P., Caubel, A., Cheruy, F., Codron, F., Cozic, A., Cugnet, D., D'Andrea, F., Davini,

P., de Lavergne, C., Denvil, S., Deshayes, J., Devilliers, M., Ducharne, A., Dufresne, J.-L., Dupont, E., Éthé, C., Fairhead, L., Falletti, L., Flavoni, S., Foujols, M.-A., Gardoll, S., Gastineau, G., Ghattas, J., Grandpeix, J.-Y., Guenet, B., Guez E., L., Guilyardi, E., Guimberteau, M., Hauglustaine, D., Hourdin, F., Idelkadi, A., Joussaume, S., Kageyama, M., Khodri, M., Krinner, G., Lebas, N., Levavasseur, G., Lévy, C., Li, L., Lott, F., Lurton, T., Luyssaert, S., Madec, G., Madeleine, J.-B., Maignan, F., Marchand, M., Marti, O., Mellul, L., Meurdesoif, Y., Mignot, J., Musat, I., Ottlé, C., Peylin, P., Planton, Y., Polcher, J., Rio, C., Rochetin, N., Rousset, C., Sepulchre, P., Sima, A., Swingedouw, D., Thiéblemont, R., Traore, A. K., Vancoppenolle, M., Vial, J., Vialard, J., Viovy, N., and Vuichard, N.: Presentation and Evaluation of the IPSL-CM6A-LR Climate Model, J. Adv. Model. Earth Syst., 12, e2019MS002010, https://doi.org/https://doi.org/10.1029/2019MS002010, 2020.

Bourgeois, T., Goris, N., Schwinger, J., and Tjiputra, J. F.: Stratification constrains future heat and carbon uptake in the Southern Ocean between 30°S and 55°S, Nat. Commun., 13, 340, https://doi.org/10.1038/s41467-022-27979-5, 2022.

Brient, F.: Reducing Uncertainties in Climate Projections with Emergent Constraints: Concepts, Examples and Prospects, Adv. Atmos. Sci., 37, 1–15, https://doi.org/10.1007/s00376-019-9140-8, 2020.

Broecker, W. S. and Peng, T.-H.: Gas exchange rates between air and sea, Tellus, 26, 21–35, https://doi.org/https://doi.org/10.1111/j.2153-3490.1974.tb01948.x, 1974.

Bronselaer, B., Winton, M., Russell, J., Sabine, C. L., and Khatiwala, S.: Agreement of CMIP5 Simulated and Observed Ocean Anthropogenic CO_2 Uptake, Geophys. Res. Lett., 44, 12, 212–298, 305, https://doi.org/https://doi.org/10.1002/2017GL074435, 2017.

Buckley, M. W. and Marshall, J.: Observations, inferences, and mechanisms of the Atlantic Meridional Overturning Circulation: A review, Rev. Geophys., 54, 5–63, https://doi.org/https://doi.org/10.1002/2015RG000493, 2016.

Bullister, J. L.: Atmospheric Histories (1765-2015) for CFC-11, CFC-12, CFC-113, CCl_4, SF_6 and N_2O (NCEI Accession 0164584).

Bushinsky, S. M., Landschützer, P., Rödenbeck, C., Gray, A. R., Baker, D., Mazloff, M. R., Resplandy, L., Johnson, K. S., and Sarmiento, J. L.: Reassessing Southern Ocean Air-Sea CO_2 Flux Estimates With the Addition of Biogeochemical Float Observations, Global Biogeochem. Cycles, 33, 1370–1388, https://doi.org/https://doi.org/10.1029/2019GB006176, 2019.

Caldeira, K. and Duffy, P. B.: The Role of the Southern Ocean in Uptake and Storage of Anthropogenic Carbon Dioxide,

Science, 287, 620–622, https://doi.org/10.1126/science.287.5453.620, 2000.

Caldwell, P. M., Bretherton, C. S., Zelinka, M. D., Klein, S. A., Santer, B. D., and Sanderson, B. M.: Statistical significance of climate sensitivity predictors obtained by data mining, Geophys. Res. Lett., 41, 1803–1808, https://doi.org/https://doi.org/10.1002/2014GL059205, 2014.

Canadell, J. G., Monteiro, P. M. S., Costa, M. H., da Cunha, L. C., Cox, P. M., Eliseev, A. V, Henson, S., Ishii, M., Jaccard, S., Koven, C., Lohila, A., Patra, P. K., Piao, S., Rogelj, J., Syampungani, S., Zaehle, S., and Zickfeld, K.: Global Carbon and other Biogeochemical Cycles and Feedbacks, 2021.

Chau, T. T. T., Gehlen, M., and Chevallier, F.: A seamless ensemble-based reconstruction of surface ocean *p*CO2 and air–sea CO_2 fluxes over the global coastal and open oceans, Biogeosciences, 19, 1087–1109, https://doi.org/10.5194/bg-19-1087-2022, 2022.

Christian, J. R., Denman, K. L., Hayashida, H., Holdsworth, A. M., Lee, W. G., Riche, O. G. J., Shao, A. E., Steiner, N., and Swart, N. C.: Ocean biogeochemistry in the Canadian Earth System Model version 5.0.3: CanESM5 and CanESM5-CanOE, Geosci. Model Dev., 15, 4393–4424, https://doi.org/10.5194/gmd-15-4393-2022, 2022.

Chylek, P., Li, J., Dubey, M. K., Wang, M., and Lesins, G.: Observed and model simulated 20th century Arctic temperature variability: Canadian Earth System Model CanESM2, Atmos. Chem. Phys. Discuss., 11, 22893–22907, https://doi.org/10.5194/acpd-11-22893-2011, 2011.

Claustre, H., Johnson, K. S., and Takeshita, Y.: Observing the Global Ocean with Biogeochemical-Argo, Ann. Rev. Mar. Sci., 12, 23–48, https://doi.org/10.1146/annurev-marine-010419-010956, 2020.

Clement, D. and Gruber, N.: The eMLR(C*) Method to Determine Decadal Changes in the Global Ocean Storage of Anthropogenic CO2, Global Biogeochem. Cycles, 32, 654–679, https://doi.org/https://doi.org/10.1002/2017GB005819, 2018.
Crisp, D., Dolman, H., Tanhua, T., McKinley, G. A., Hauck, J., Bastos, A., Sitch, S., Eggleston, S., and Aich, V.: How Well Do We Understand the Land-Ocean-Atmosphere Carbon Cycle?, Rev. Geophys., 60, e2021RG000736, https://doi.org/https://doi.org/10.1029/2021RG000736, 2022.

Danabasoglu, G., Lamarque, J.-F., Bacmeister, J., Bailey, D. A., DuVivier, A. K., Edwards, J., Emmons, L. K., Fasullo, J., Garcia, R., Gettelman, A., Hannay, C., Holland, M. M., Large, W. G., Lauritzen, P. H., Lawrence, D. M., Lenaerts, J. T. M., Lindsay, K., Lipscomb, W. H., Mills, M. J., Neale, R., Oleson, K. W., Otto-Bliesner, B., Phillips, A. S., Sacks, W., Tilmes, S.,

https://doi.org/10.5194/bg-2022-134
Preprint. Discussion started: 20 June 2022

van Kampenhout, L., Vertenstein, M., Bertini, A., Dennis, J., Deser, C., Fischer, C., Fox-Kemper, B., Kay, J. E., Kinnison, D., Kushner, P. J., Larson, V. E., Long, M. C., Mickelson, S., Moore, J. K., Nienhouse, E., Polvani, L., Rasch, P. J., and Strand, W. G.: The Community Earth System Model Version 2 (CESM2), J. Adv. Model. Earth Syst., 12, https://doi.org/https://doi.org/10.1029/2019MS001916, 2020.

DeVries, T.: The oceanic anthropogenic CO_2 sink: Storage, air-sea fluxes, and transports over the industrial era, Global Biogeochem. Cycles, 28, 631–647, https://doi.org/https://doi.org/10.1002/2013GB004739, 2014.

Dickson, A. G., Sabine, C. L., and Christian, J. R.: Guide to best practices for ocean CO_2 measurements., North Pacific Marine Science Organization, 2007.

Trends in Atmospheric Carbon Dioxide (NOAA/GML)

Doney, S. C., Busch, D. S., Cooley, S. R., and Kroeker, K. J.: The Impacts of Ocean Acidification on Marine Ecosystems and Reliant Human Communities, Annu. Rev. Environ. Resour., 45, 83–112, https://doi.org/10.1146/annurev-environ-012320-083019, 2020.

Döscher, R., Acosta, M., Alessandri, A., Anthoni, P., Arsouze, T., Bergman, T., Bernardello, R., Boussetta, S., Caron, L.-P., Carver, G., Castrillo, M., Catalano, F., Cvijanovic, I., Davini, P., Dekker, E., Doblas-Reyes, F. J., Docquier, D., Echevarria, P., Fladrich, U., Fuentes-Franco, R., Gröger, M., v. Hardenberg, J., Hieronymus, J., Karami, M. P., Keskinen, J.-P., Koenigk, T., Makkonen, R., Massonnet, F., Ménégoz, M., Miller, P. A., Moreno-Chamarro, E., Nieradzik, L., van Noije, T., Nolan, P., O'Donnell, D., Ollinaho, P., van den Oord, G., Ortega, P., Prims, O. T., Ramos, A., Reerink, T., Rousset, C., Ruprich-Robert, Y., Le Sager, P., Schmith, T., Schrödner, R., Serva, F., Sicardi, V., Sloth Madsen, M., Smith, B., Tian, T., Tourigny, E., Uotila, P., Vancoppenolle, M., Wang, S., Wårlind, D., Willén, U., Wyser, K., Yang, S., Yepes-Arbós, X., and Zhang, Q.: The EC-Earth3 Earth system model for the Coupled Model IntercomparisonProject 6, Geosci. Model Dev., 15, 2973–3020, https://doi.org/10.5194/gmd-15-2973-2022, 2022.

Dunne, J. P., John, J. G., Adcroft, A. J., Griffies, S. M., Hallberg, R. W., Shevliakova, E., Stouffer, R. J., Cooke, W., Dunne, K. A., Harrison, M. J., Krasting, J. P., Malyshev, S. L., Milly, P. C. D., Phillipps, P. J., Sentman, L. T., Samuels, B. L., Spelman, M. J., Winton, M., Wittenberg, A. T., and Zadeh, N.: GFDL's ESM2 Global Coupled Climate–Carbon Earth System Models. Part I: Physical Formulation and Baseline Simulation Characteristics, J. Clim., 25, 6646–6665, https://doi.org/10.1175/JCLI-D-11-00560.1, 2012.

Dunne, J. P., Horowitz, L. W., Adcroft, A. J., Ginoux, P., Held, I. M., John, J. G., Krasting, J. P., Malyshev, S., Naik, V.,

https://doi.org/10.5194/bg-2022-134
Preprint. Discussion started: 20 June 2022

Paulot, F., Shevliakova, E., Stock, C. A., Zadeh, N., Balaji, V., Blanton, C., Dunne, K. A., Dupuis, C., Durachta, J., Dussin, R., Gauthier, P. P. G., Griffies, S. M., Guo, H., Hallberg, R. W., Harrison, M., He, J., Hurlin, W., McHugh, C., Menzel, R., Milly, P. C. D., Nikonov, S., Paynter, D. J., Ploshay, J., Radhakrishnan, A., Rand, K., Reichl, B. G., Robinson, T., Schwarzkopf, D. M., Sentman, L. T., Underwood, S., Vahlenkamp, H., Winton, M., Wittenberg, A. T., Wyman, B., Zeng, Y., and Zhao, M.: The GFDL Earth System Model Version 4.1 (GFDL-ESM 4.1): Overall Coupled Model Description and Simulation Characteristics, J. Adv. Model. Earth Syst., 12, e2019MS002015, https://doi.org/https://doi.org/10.1029/2019MS002015, 2020.

Eyring, V., Cox, P. M., Flato, G. M., Gleckler, P. J., Abramowitz, G., Caldwell, P., Collins, W. D., Gier, B. K., Hall, A. D., Hoffman, F. M., Hurtt, G. C., Jahn, A., Jones, C. D., Klein, S. A., Krasting, J. P., Kwiatkowski, L., Lorenz, R., Maloney, E., Meehl, G. A., Pendergrass, A. G., Pincus, R., Ruane, A. C., Russell, J. L., Sanderson, B. M., Santer, B. D., Sherwood, S. C., Simpson, I. R., Stouffer, R. J., and Williamson, M. S.: Taking climate model evaluation to the next level, Nat. Clim. Chang., 9, 102–110, https://doi.org/10.1038/s41558-018-0355-y, 2019.

Fabry, V. J., Seibel, B. A., Feely, R. A., and Orr, J. C.: Impacts of ocean acidification on marine fauna and ecosystem processes, ICES J. Mar. Sci., 65, 414–432, https://doi.org/10.1093/icesjms/fsn048, 2008.

Falkowski, P. G., Barber, R. T., and Smetacek, V.: Biogeochemical Controls and Feedbacks on Ocean Primary Production, Science, 281, 200–206, https://doi.org/10.1126/science.281.5374.200, 1998.

Friedlingstein, P., Jones, M. W., O'Sullivan, M., Andrew, R. M., Bakker, D. C. E., Hauck, J., Le Quéré, C., Peters, G. P., Peters, W., Pongratz, J., Sitch, S., Canadell, J. G., Ciais, P., Jackson, R. B., Alin, S. R., Anthoni, P., Bates, N. R., Becker, M., Bellouin, N., Bopp, L., Chau, T. T. T., Chevallier, F., Chini, L. P., Cronin, M., Currie, K. I., Decharme, B., Djeutchouang, L. M., Dou, X., Evans, W., Feely, R. A., Feng, L., Gasser, T., Gilfillan, D., Gkritzalis, T., Grassi, G., Gregor, L., Gruber, N., Gürses, Ö., Harris, I., Houghton, R. A., Hurtt, G. C., Iida, Y., Ilyina, T., Luijkx, I. T., Jain, A., Jones, S. D., Kato, E., Kennedy, D., Klein Goldewijk, K., Knauer, J., Korsbakken, J. I., Körtzinger, A., Landschützer, P., Lauvset, S. K., Lefèvre, N., Lienert, S., Liu, J., Marland, G., McGuire, P. C., Melton, J. R., Munro, D. R., Nabel, J. E. M. S., Nakaoka, S.-I., Niwa, Y., Ono, T., Pierrot, D., Poulter, B., Rehder, G., Resplandy, L., Robertson, E., Rödenbeck, C., Rosan, T. M., Schwinger, J., Schwingshackl, C., Séférian, R., Sutton, A. J., Sweeney, C., Tanhua, T., Tans, P. P., Tian, H., Tilbrook, B., Tubiello, F., van der Werf, G. R., Vuichard, N., Wada, C., Wanninkhof, R., Watson, A. J., Willis, D., Wiltshire, A. J., Yuan, W., Yue, C., Yue, X., Zaehle, S., and Zeng, J.: Global Carbon Budget 2021, Earth Syst. Sci. Data, 14, 1917–2005, https://doi.org/10.5194/essd-14-1917-2022, 2022.

Frölicher, T. L. and Joos, F.: Reversible and irreversible impacts of greenhouse gas emissions in multi-century projections

with the NCAR global coupled carbon cycle-climate model, Clim. Dyn., 35, 1439–1459, https://doi.org/10.1007/s00382-009-0727-0, 2010.

Frölicher, T. L., Sarmiento, J. L., Paynter, D. J., Dunne, J. P., Krasting, J. P., and Winton, M.: Dominance of the Southern Ocean in Anthropogenic Carbon and Heat Uptake in CMIP5 Models, J. Clim., 28, 862–886, https://doi.org/10.1175/JCLI-D-14-00117.1, 2015.

Gangstø, R., Gehlen, M., Schneider, B., Bopp, L., Aumont, O., and Joos, F.: Modeling the marine aragonite cycle: changes under rising carbon dioxide and its role in shallow water $CaCO_3$ dissolution, Biogeosciences, 5, 1057–1072, https://doi.org/10.5194/bg-5-1057-2008, 2008.

Gattuso, J.-P. and Hansson, L.: Ocean acidification, Oxford University Press, 2011.

Gent, P. R., Danabasoglu, G., Donner, L. J., Holland, M. M., Hunke, E. C., Jayne, S. R., Lawrence, D. M., Neale, R. B., Rasch, P. J., Vertenstein, M., Worley, P. H., Yang, Z.-L., and Zhang, M.: The Community Climate System Model Version 4, J. Clim., 24, 4973–4991, https://doi.org/10.1175/2011JCLI4083.1, 2011.

Gerber, M., Joos, F., Vázquez-Rodríguez, M., Touratier, F., and Goyet, C.: Regional air-sea fluxes of anthropogenic carbon inferred with an Ensemble Kalman Filter, Global Biogeochem. Cycles, 23, https://doi.org/https://doi.org/10.1029/2008GB003247, 2009.

Giorgetta, M. A., Jungclaus, J., Reick, C. H., Legutke, S., Bader, J., Böttinger, M., Brovkin, V., Crueger, T., Esch, M., Fieg, K., Glushak, K., Gayler, V., Haak, H., Hollweg, H.-D., Ilyina, T., Kinne, S., Kornblueh, L., Matei, D., Mauritsen, T., Mikolajewicz, U., Mueller, W., Notz, D., Pithan, F., Raddatz, T., Rast, S., Redler, R., Roeckner, E., Schmidt, H., Schnur, R., Segschneider, J., Six, K. D., Stockhause, M., Timmreck, C., Wegner, J., Widmann, H., Wieners, K.-H., Claussen, M., Marotzke, J., and Stevens, B.: Climate and carbon cycle changes from 1850 to 2100 in MPI-ESM simulations for the Coupled Model Intercomparison Project phase 5, J. Adv. Model. Earth Syst., 5, 572–597, https://doi.org/https://doi.org/10.1002/jame.20038, 2013.

Gloege, L., McKinley, G. A., Landschützer, P., Fay, A. R., Frölicher, T. L., Fyfe, J. C., Ilyina, T., Jones, S., Lovenduski, N. S., Rodgers, K. B., Schlunegger, S., and Takano, Y.: Quantifying Errors in Observationally Based Estimates of Ocean Carbon Sink Variability, Global Biogeochem. Cycles, 35, e2020GB006788, https://doi.org/https://doi.org/10.1029/2020GB006788, 2021.

Gloege, L., Yan, M., Zheng, T., and McKinley, G. A.: Improved Quantification of Ocean Carbon Uptake by Using Machine Learning to Merge Global Models and pCO_2 Data, J. Adv. Model. Earth Syst., 14, e2021MS002620, https://doi.org/https://doi.org/10.1029/2021MS002620, 2022.

Goris, N., Tjiputra, J. F., Olsen, A., Schwinger, J., Lauvset, S. K., and Jeansson, E.: Constraining Projection-Based Estimates of the Future North Atlantic Carbon Uptake, J. Clim., 31, 3959–3978, https://doi.org/10.1175/JCLI-D-17-0564.1, 2018.

Gregor, L. and Gruber, N.: OceanSODA-ETHZ: a global gridded data set of the surface ocean carbonate system for seasonal to decadal studies of ocean acidification, Earth Syst. Sci. Data, 13, 777–808, https://doi.org/10.5194/essd-13-777-2021, 2021.

Gregor, L., Lebehot, A. D., Kok, S., and Scheel Monteiro, P. M.: A comparative assessment of the uncertainties of global surface ocean CO_2 estimates using a machine-learning ensemble (CSIR-ML6 version2019a) – have we hit the wall?, Geosci. Model Dev., 12, 5113–5136, https://doi.org/10.5194/gmd-12-5113-2019, 2019.

Gruber, N., Sarmiento, J. L., and Stocker, T. F.: An improved method for detecting anthropogenic CO_2 in the oceans, Global Biogeochem. Cycles, 10, 809–837, https://doi.org/https://doi.org/10.1029/96GB01608, 1996.

Gruber, N., Gloor, M., Mikaloff Fletcher, S. E., Doney, S. C., Dutkiewicz, S., Follows, M. J., Gerber, M., Jacobson, A. R., Joos, F., Lindsay, K., Menemenlis, D., Mouchet, A., Müller, S. A., Sarmiento, J. L., and Takahashi, T.: Oceanic sources, sinks, and transport of atmospheric CO_2, Global Biogeochem. Cycles, 23, https://doi.org/https://doi.org/10.1029/2008GB003349, 2009.

Gruber, N., Hauri, C., Lachkar, Z., Loher, D., Frölicher, T. L., and Plattner, G.-K.: Rapid Progression of Ocean Acidification in the California Current System, Science, 337, 220–223, https://doi.org/10.1126/science.1216773, 2012.

Gruber, N., Clement, D., Carter, B. R., Feely, R. A., van Heuven, S., Hoppema, M., Ishii, M., Key, R. M., Kozyr, A., Lauvset, S. K., Lo Monaco, C., Mathis, J. T., Murata, A., Olsen, A., Perez, F. F., Sabine, C. L., Tanhua, T., and Rik, W.: The oceanic sink for anthropogenic CO_2 from 1994 to 2007, Science, 363, 1193–1199, https://doi.org/10.1126/science.aau5153, 2019a.

Gruber, N., Landschützer, P., and Lovenduski, N. S.: The Variable Southern Ocean Carbon Sink, Ann. Rev. Mar. Sci., 11, 159–186, https://doi.org/10.1146/annurev-marine-121916-063407, 2019b.

Gutjahr, O., Putrasahan, D., Lohmann, K., Jungclaus, J. H., von Storch, J.-S., Brüggemann, N., Haak, H., and Stössel, A.: Max Planck Institute Earth System Model (MPI-ESM1.2) for the High-Resolution Model Intercomparison Project (HighResMIP), Geosci. Model Dev., 12, 3241–3281, https://doi.org/10.5194/gmd-12-3241-2019, 2019.

Hajima, T., Watanabe, M., Yamamoto, A., Tatebe, H., Noguchi, M. A., Abe, M., Ohgaito, R., Ito, A., Yamazaki, D., Okajima, H., Ito, A., Takata, K., Ogochi, K., Watanabe, S., and Kawamiya, M.: Development of the MIROC-ES2L Earth system model and the evaluation of biogeochemical processes and feedbacks, Geosci. Model Dev., 13, 2197–2244, https://doi.org/10.5194/gmd-13-2197-2020, 2020.

Hall, A., Cox, P., Huntingford, C., and Klein, S.: Progressing emergent constraints on future climate change, Nat. Clim. Chang., 9, 269–278, https://doi.org/10.1038/s41558-019-0436-6, 2019.

Hall, T. M., Haine, T. W. N., and Waugh, D. W.: Inferring the concentration of anthropogenic carbon in the ocean from tracers, Global Biogeochem. Cycles, 16, 78-1-78–15, https://doi.org/https://doi.org/10.1029/2001GB001835, 2002.

Hauck, J. and Völker, C.: Rising atmospheric CO_2 leads to large impact of biology on Southern Ocean CO_2 uptake via changes of the Revelle factor, Geophys. Res. Lett., 42, 1459–1464, https://doi.org/https://doi.org/10.1002/2015GL063070, 2015.

Hauck, J., Zeising, M., Le Quéré, C., Gruber, N., Bakker, D. C. E., Bopp, L., Chau, T. T. T., Gürses, Ö., Ilyina, T., Landschützer, P., Lenton, A., Resplandy, L., Rödenbeck, C., Schwinger, J., and Séférian, R.: Consistency and Challenges in the Ocean Carbon Sink Estimate for the Global Carbon Budget, Front. Mar. Sci., 7, https://doi.org/10.3389/fmars.2020.571720, 2020.

Hauri, C., Pagès, R., McDonnell, A. M. P., Stuecker, M. F., Danielson, S. L., Hedstrom, K., Irving, B., Schultz, C., and Doney, S. C.: Modulation of ocean acidification by decadal climate variability in the Gulf of Alaska, Commun. Earth Environ., 2, 191, https://doi.org/10.1038/s43247-021-00254-z, 2021.

Hausfather, Z., Marvel, K., Schmidt, G. A., Nielsen-Gammon, J. W., and Zelinka, M.: Climate simulations: recognize the 'hot model' problem, Nature, 605, 26–29, https://doi.org/10.1038/d41586-022-01192-2, 2022.

Held, I. M., Guo, H., Adcroft, A., Dunne, J. P., Horowitz, L. W., Krasting, J., Shevliakova, E., Winton, M., Zhao, M., Bushuk, M., Wittenberg, A. T., Wyman, B., Xiang, B., Zhang, R., Anderson, W., Balaji, V., Donner, L., Dunne, K., Durachta, J., Gauthier, P. P. G., Ginoux, P., Golaz, J.-C., Griffies, S. M., Hallberg, R., Harris, L., Harrison, M., Hurlin, W., John, J., Lin, P., Lin, S.-J., Malyshev, S., Menzel, R., Milly, P. C. D., Ming, Y., Naik, V., Paynter, D., Paulot, F., Ramaswamy, V., Reichl, B., Robinson, T., Rosati, A., Seman, C., Silvers, L. G., Underwood, S., and Zadeh, N.: Structure and Performance of GFDL's CM4.0 Climate Model, J. Adv. Model. Earth Syst., 11, 3691–3727, https://doi.org/https://doi.org/10.1029/2019MS001829, 2019.

https://doi.org/10.5194/bg-2022-134
Preprint. Discussion started: 20 June 2022

Hess, D.: Constraining the anthropogenic carbon uptake in the North Atlantic over the 21st century, University of Bern, 1–45 pp., 2022.

Iida, Y., Takatani, Y., Kojima, A., and Ishii, M.: Global trends of ocean CO_2 sink and ocean acidification: an observation-based reconstruction of surface ocean inorganic carbon variables, J. Oceanogr., 77, 323–358, https://doi.org/10.1007/s10872-020-00571-5, 2021.

IPCC: Summary for Policymakers, in: Climate Change 2021: The Physical Science Basis. Contribution of Working Group I to the Sixth Assessment Report of the Intergovernmental Panel on Climate Change, edited by: Masson-Delmotte, V., Zhai, P., Pirani, A., Connors, S. L., Péan, C., Berger, S., Caud, N., Chen, Y., Goldfarb, L., Gomis, M. I., Huang, M., Leitzell, K., Lonnoy, E., Matthews, J. B. R., Maycock, T. K., Waterfield, T., Yelekçi, O., Yu, R., and Zhou, B., Cambridge University Press, 2021.

IPCC: Climate Change 2022: Mitigation of Climate Change. Contribution of Working Group III to the Sixth Assessment Report of the Intergovernmental Panel on Climate Change, edited by: Shukla, P. R., Skea, J., Slade, R., Al Khourdajie, A., van Diemen, R., McCollum, D., Pathak, M., Some, S., Vyas, P., Fradera, R., Belkacemi, M., Hasija, A., Lisboa, G., Luz, S., and Malley, J., Cambridge University Press, Cambridge, UK and New York, NY, 2022.

Jacobson, A. R., Mikaloff Fletcher, S. E., Gruber, N., Sarmiento, J. L., and Gloor, M.: A joint atmosphere-ocean inversion for surface fluxes of carbon dioxide: 1. Methods and global-scale fluxes, Global Biogeochem. Cycles, 21, https://doi.org/https://doi.org/10.1029/2005GB002556, 2007.

Joos, F., Plattner, G.-K., Stocker, T. F., Marchal, O., and Schmittner, A.: Global Warming and Marine Carbon Cycle Feedbacks on Future Atmospheric CO_2, Science, 284, 464–467, https://doi.org/10.1126/science.284.5413.464, 1999.

Kawaguchi, S., Ishida, A., King, R., Raymond, B., Waller, N., Constable, A., Nicol, S., Wakita, M., and Ishimatsu, A.: Risk maps for Antarctic krill under projected Southern Ocean acidification, Nat. Clim. Chang., 3, 843–847, https://doi.org/10.1038/nclimate1937, 2013.

Khatiwala, S., Tanhua, T., Mikaloff Fletcher, S., Gerber, M., Doney, S. C., Graven, H. D., Gruber, N., McKinley, G. A., Murata, A., Rios, A. F., and Sabine, C. L.: Global ocean storage of anthropogenic carbon, Biogeosciences, 10, 2169–2191, https://doi.org/10.5194/bg-10-2169-2013, 2013.

Kroeker, K. J., Kordas, R. L., Crim, R. N., and Singh, G. G.: Meta-analysis reveals negative yet variable effects of ocean

acidification on marine organisms, Ecol. Lett., 13, 1419–1434, https://doi.org/https://doi.org/10.1111/j.1461-0248.2010.01518.x, 2010.

Kroeker, K. J., Kordas, R. L., Crim, R., Hendriks, I. E., Ramajo, L., Singh, G. S., Duarte, C. M., and Gattuso, J.-P.: Impacts of ocean acidification on marine organisms: quantifying sensitivities and interaction with warming, Glob. Chang. Biol., 19, 1884–1896, https://doi.org/https://doi.org/10.1111/gcb.12179, 2013.

Kwiatkowski, L., Bopp, L., Aumont, O., Ciais, P., Cox, P. M., Laufkötter, C., Li, Y., and Séférian, R.: Emergent constraints on projections of declining primary production in the tropical oceans, Nat. Clim. Chang., 7, 355–358, https://doi.org/10.1038/nclimate3265, 2017.

Kwiatkowski, L., Torres, O., Bopp, L., Aumont, O., Chamberlain, M., Christian, J. R., Dunne, J. P., Gehlen, M., Ilyina, T., John, J. G., Lenton, A., Li, H., Lovenduski, N. S., Orr, J. C., Palmieri, J., Santana-Falcón, Y., Schwinger, J., Séférian, R., Stock, C. A., Tagliabue, A., Takano, Y., Tjiputra, J., Toyama, K., Tsujino, H., Watanabe, M., Yamamoto, A., Yool, A., and Ziehn, T.: Twenty-first century ocean warming, acidification, deoxygenation, and upper-ocean nutrient and primary production decline from CMIP6 model projections, Biogeosciences, 17, 3439–3470, https://doi.org/10.5194/bg-17-3439-2020, 2020.

Kwon, E. Y., Primeau, F., and Sarmiento, J. L.: The impact of remineralization depth on the air–sea carbon balance, Nat. Geosci., 2, 630–635, https://doi.org/10.1038/ngeo612, 2009.

Lacroix, F., Ilyina, T., and Hartmann, J.: Oceanic CO_2 outgassing and biological production hotspots induced by pre-industrial river loads of nutrients and carbon in a global modeling approach, Biogeosciences, 17, 55–88, https://doi.org/10.5194/bg-17-55-2020, 2020.

Landschützer, P., Gruber, N., and Bakker, D. C. E.: Decadal variations and trends of the global ocean carbon sink, Global Biogeochem. Cycles, 30, 1396–1417, https://doi.org/https://doi.org/10.1002/2015GB005359, 2016.

Langdon, C. and Atkinson, M. J.: Effect of elevated pCO_2 on photosynthesis and calcification of corals and interactions with seasonal change in temperature/irradiance and nutrient enrichment, J. Geophys. Res. Ocean., 110, https://doi.org/https://doi.org/10.1029/2004JC002576, 2005.

Lauvset, S. K., Key, R. M., Olsen, A., van Heuven, S., Velo, A., Lin, X., Schirnick, C., Kozyr, A., Tanhua, T., Hoppema, M., Jutterström, S., Steinfeldt, R., Jeansson, E., Ishii, M., Perez, F. F., Suzuki, T., and Watelet, S.: A new global interior ocean mapped climatology: the 11 GLODAP version 2, Earth Syst. Sci. Data, 8, 325–340, https://doi.org/10.5194/essd-8-325-2016,

2016.

Lauvset, S. K., Lange, N., Tanhua, T., Bittig, H. C., Olsen, A., Kozyr, A., Álvarez, M., Becker, S., Brown, P. J., Carter, B. R., da Cunha, L., Feely, R. A., van Heuven, S., Hoppema, M., Ishii, M., Jeansson, E., Jutterström, S., Jones, S. D., Karlsen, M. K., Lo Monaco, C., Michaelis, P., Murata, A., Pérez, F. F., Pfeil, B., Schirnick, C., Steinfeldt, R., Suzuki, T., Tilbrook, B., Velo, A., Wanninkhof, R., Woosley, R. J., and Key, R. M.: An updated version of the global interior ocean biogeochemical data product, GLODAPv2.2021, Earth Syst. Sci. Data, 13, 5565–5589, https://doi.org/10.5194/essd-13-5565-2021, 2021.

Lebrato, M., Andersson, A. J., Ries, J. B., Aronson, R. B., Lamare, M. D., Koeve, W., Oschlies, A., Iglesias-Rodriguez, M. D., Thatje, S., Amsler, M., Vos, S. C., Jones, D. O. B., Ruhl, H. A., Gates, A. R., and McClintock, J. B.: Benthic marine calcifiers coexist with $CaCO_3$-undersaturated seawater worldwide, Global Biogeochem. Cycles, 30, 1038–1053, https://doi.org/https://doi.org/10.1002/2015GB005260, 2016.

Lindsay, K., Bonan, G. B., Doney, S. C., Hoffman, F. M., Lawrence, D. M., Long, M. C., Mahowald, N. M., Keith Moore, J., Randerson, J. T., and Thornton, P. E.: Preindustrial-Control and Twentieth-Century Carbon Cycle Experiments with the Earth System Model CESM1(BGC), J. Clim., 27, 8981–9005, https://doi.org/10.1175/JCLI-D-12-00565.1, 2014.

Locarnini, R. A., Mishonov, A. V., Baranova, O. K., Boyer, T. P., Zweng, M. M., Garcia, H. E., Reagan, J. R., Seidov, D., Weathers, K., Paver, C. R., and Smolyar, I.: World Ocean Atlas 2018, Volume 1: Temperature, NOAA Atlas NESDIS 82, 2018.

Lovato, T., Peano, D., Butenschön, M., Materia, S., Iovino, D., Scoccimarro, E., Fogli, P. G., Cherchi, A., Bellucci, A., Gualdi, S., Masina, S., and Navarra, A.: CMIP6 Simulations With the CMCC Earth System Model (CMCC-ESM2), J. Adv. Model. Earth Syst., 14, e2021MS002814, https://doi.org/https://doi.org/10.1029/2021MS002814, 2022.

Marshall, J. and Speer, K.: Closure of the meridional overturning circulation through Southern Ocean upwelling, Nat. Geosci., 5, 171–180, https://doi.org/10.1038/ngeo1391, 2012.

Matear, R. J., Wong, C. S., and Xie, L.: Can CFCs be used to determine anthropogenic CO_2?, Global Biogeochem. Cycles, 17, https://doi.org/https://doi.org/10.1029/2001GB001415, 2003.

Matsumoto, K., Sarmiento, J. L., Key, R. M., Aumont, O., Bullister, J. L., Caldeira, K., Campin, J.-M., Doney, S. C., Drange, H., Dutay, J.-C., Follows, M., Gao, Y., Gnanadesikan, A., Gruber, N., Ishida, A., Joos, F., Lindsay, K., Maier-Reimer, E., Marshall, J. C., Matear, R. J., Monfray, P., Mouchet, A., Najjar, R., Plattner, G.-K., Schlitzer, R., Slater, R., Swathi, P. S.,

Totterdell, I. J., Weirig, M.-F., Yamanaka, Y., Yool, A., and Orr, J. C.: Evaluation of ocean carbon cycle models with data-based metrics, Geophys. Res. Lett., 31, https://doi.org/https://doi.org/10.1029/2003GL018970, 2004.

Mauritsen, T., Bader, J., Becker, T., Behrens, J., Bittner, M., Brokopf, R., Brovkin, V., Claussen, M., Crueger, T., Esch, M., Fast, I., Fiedler, S., Fläschner, D., Gayler, V., Giorgetta, M., Goll, D. S., Haak, H., Hagemann, S., Hedemann, C., Hohenegger, C., Ilyina, T., Jahns, T., Jimenéz-de-la-Cuesta, D., Jungclaus, J., Kleinen, T., Kloster, S., Kracher, D., Kinne, S., Kleberg, D., Lasslop, G., Kornblueh, L., Marotzke, J., Matei, D., Meraner, K., Mikolajewicz, U., Modali, K., Möbis, B., Müller, W. A., Nabel, J. E. M. S., Nam, C. C. W., Notz, D., Nyawira, S.-S., Paulsen, H., Peters, K., Pincus, R., Pohlmann, H., Pongratz, J., Popp, M., Raddatz, T. J., Rast, S., Redler, R., Reick, C. H., Rohrschneider, T., Schemann, V., Schmidt, H., Schnur, R., Schulzweida, U., Six, K. D., Stein, L., Stemmler, I., Stevens, B., von Storch, J.-S., Tian, F., Voigt, A., Vrese, P., Wieners, K.-H., Wilkenskjeld, S., Winkler, A., and Roeckner, E.: Developments in the MPI-M Earth System Model version 1.2 (MPI-ESM1.2) and Its Response to Increasing CO_2, J. Adv. Model. Earth Syst., 11, 998–1038, https://doi.org/https://doi.org/10.1029/2018MS001400, 2019.

McCarthy, G. D., Brown, P. J., Flagg, C. N., Goni, G., Houpert, L., Hughes, C. W., Hummels, R., Inall, M., Jochumsen, K., Larsen, K. M. H., Lherminier, P., Meinen, C. S., Moat, B. I., Rayner, D., Rhein, M., Roessler, A., Schmid, C., and Smeed, D. A.: Sustainable Observations of the AMOC: Methodology and Technology, Rev. Geophys., 58, e2019RG000654, https://doi.org/https://doi.org/10.1029/2019RG000654, 2020.

McKinley, G. A., Fay, A. R., Eddebbar, Y. A., Gloege, L., and Lovenduski, N. S.: External Forcing Explains Recent Decadal Variability of the Ocean Carbon Sink, AGU Adv., 1, e2019AV000149, https://doi.org/https://doi.org/10.1029/2019AV000149, 2020.

McNeil, B. I. and Matear, R. J.: The non-steady state oceanic CO_2 signal: its importance, magnitude and a novel way to detect it, Biogeosciences, 10, 2219–2228, https://doi.org/10.5194/bg-10-2219-2013, 2013.

Meinshausen, M., Nicholls, Z. R. J., Lewis, J., Gidden, M. J., Vogel, E., Freund, M., Beyerle, U., Gessner, C., Nauels, A., Bauer, N., Canadell, J. G., Daniel, J. S., John, A., Krummel, P. B., Luderer, G., Meinshausen, N., Montzka, S. A., Rayner, P. J., Reimann, S., Smith, S. J., van den Berg, M., Velders, G. J. M., Vollmer, M. K., and Wang, R. H. J.: The shared socio-economic pathway (SSP) greenhouse gas concentrations and their extensions to 2500, Geosci. Model Dev., 13, 3571–3605, https://doi.org/10.5194/gmd-13-3571-2020, 2020.

Mikaloff Fletcher, S. E., Gruber, N., Jacobson, A. R., Doney, S. C., Dutkiewicz, S., Gerber, M., Follows, M., Joos, F., Lindsay, K., Menemenlis, D., Mouchet, A., Müller, S. A., and Sarmiento, J. L.: Inverse estimates of anthropogenic CO2 uptake,

transport, and storage by the ocean, Global Biogeochem. Cycles, 20, https://doi.org/https://doi.org/10.1029/2005GB002530, 2006.

Morrison, A. K., Frölicher, T. L., and Sarmiento, J. L.: Upwelling in the Southern Ocean, Phys. Today, 68, 27–32, https://doi.org/10.1063/PT.3.2654, 2015.

O'Neill, B. C., Tebaldi, C., van Vuuren, D. P., Eyring, V., Friedlingstein, P., Hurtt, G., Knutti, R., Kriegler, E., Lamarque, J.-F., Lowe, J., Meehl, G. A., Moss, R., Riahi, K., and Sanderson, B. M.: The Scenario Model Intercomparison Project (ScenarioMIP) for CMIP6, Geosci. Model Dev., 9, 3461–3482, https://doi.org/10.5194/gmd-9-3461-2016, 2016.

Orr, J. C.: Global Ocean Storage of Anthropogenic Carbon, Inst. Pierre Simon Laplace, Gif-sur-Yvette, France, 116 pp pp., 2002.

Orr, J. C. and Epitalon, J.-M.: Improved routines to model the ocean carbonate system: mocsy 2.0, Geosci. Model Dev., 8, 485–499, https://doi.org/10.5194/gmd-8-485-2015, 2015.

Orr, J. C., Fabry, V. J., Aumont, O., Bopp, L., Doney, S. C., Feely, R. A., Gnanadesikan, A., Gruber, N., Ishida, A., Joos, F., Key, R. M., Lindsay, K., Maier-Reimer, E., Matear, R., Monfray, P., Mouchet, A., Najjar, R. G., Plattner, G.-K., Rodgers, K. B., Sabine, C. L., Sarmiento, J. L., Schlitzer, R., Slater, R. D., Totterdell, I. J., Weirig, M.-F., Yamanaka, Y., and Yool, A.: Anthropogenic ocean acidification over the twenty-first century and its impact on calcifying organisms, Nature, 437, 681–686, https://doi.org/10.1038/nature04095, 2005.

Pérez, F. F., Mercier, H., Vázquez-Rodríguez, M., Lherminier, P., Velo, A., Pardo, P. C., Rosón, G., and Ríos, A. F.: Atlantic Ocean CO_2 uptake reduced by weakening of the meridional overturning circulation, Nat. Geosci., 6, 146–152, https://doi.org/10.1038/ngeo1680, 2013.

Plattner, G.-K., Joos, F., Stocker, T. F., and Marchal, O.: Feedback mechanisms and sensitivities of ocean carbon uptake under global warming, Tellus B Chem. Phys. Meteorol., 53, 564–592, https://doi.org/10.3402/tellusb.v53i5.16637, 2001.

Regnier, P., Resplandy, L., Najjar, R. G., and Ciais, P.: The land-to-ocean loops of the global carbon cycle, Nature, 603, 401–410, https://doi.org/10.1038/s41586-021-04339-9, 2022.

Resplandy, L., Keeling, R. F., Rödenbeck, C., Stephens, B. B., Khatiwala, S., Rodgers, K. B., Long, M. C., Bopp, L., and Tans, P. P.: Revision of global carbon fluxes based on a reassessment of oceanic and riverine carbon transport, Nat. Geosci.,

11, 504–509, https://doi.org/10.1038/s41561-018-0151-3, 2018.

Revelle, R. and Suess, H. E.: Carbon Dioxide Exchange Between Atmosphere and Ocean and the Question of an Increase of Atmospheric CO_2 during the Past Decades, Tellus, 9, 18–27, https://doi.org/https://doi.org/10.1111/j.2153-3490.1957.tb01849.x, 1957.

Riahi, K., van Vuuren, D. P., Kriegler, E., Edmonds, J., O'Neill, B. C., Fujimori, S., Bauer, N., Calvin, K., Dellink, R., Fricko, O., Lutz, W., Popp, A., Cuaresma, J. C., KC, S., Leimbach, M., Jiang, L., Kram, T., Rao, S., Emmerling, J., Ebi, K., Hasegawa, T., Havlik, P., Humpenöder, F., Da Silva, L. A., Smith, S., Stehfest, E., Bosetti, V., Eom, J., Gernaat, D., Masui, T., Rogelj, J., Strefler, J., Drouet, L., Krey, V., Luderer, G., Harmsen, M., Takahashi, K., Baumstark, L., Doelman, J. C., Kainuma, M., Klimont, Z., Marangoni, G., Lotze-Campen, H., Obersteiner, M., Tabeau, A., and Tavoni, M.: The Shared Socioeconomic Pathways and their energy, land use, and greenhouse gas emissions implications: An overview, Glob. Environ. Chang., 42, 153–168, https://doi.org/https://doi.org/10.1016/j.gloenvcha.2016.05.009, 2017.

Ridge, S. M. and McKinley, G. A.: Advective Controls on the North Atlantic Anthropogenic Carbon Sink, Global Biogeochem. Cycles, 34, e2019GB006457, https://doi.org/https://doi.org/10.1029/2019GB006457, 2020.

Riebesell, U., Schulz, K. G., Bellerby, R. G. J., Botros, M., Fritsche, P., Meyerhöfer, M., Neill, C., Nondal, G., Oschlies, A., Wohlers, J., and Zöllner, E.: Enhanced biological carbon consumption in a high CO_2 ocean, Nature, 450, 545–548, https://doi.org/10.1038/nature06267, 2007.

Ries, J. B., Cohen, A. L., and McCorkle, D. C.: Marine calcifiers exhibit mixed responses to CO_2-induced ocean acidification, Geology, 37, 1131–1134, https://doi.org/10.1130/G30210A.1, 2009.

Rödenbeck, C., Bakker, D. C. E., Metzl, N., Olsen, A., Sabine, C., Cassar, N., Reum, F., Keeling, R. F., and Heimann, M.: Interannual sea–air CO_2 flux variability from an observation-driven ocean mixed-layer scheme, Biogeosciences, 11, 4599–4613, https://doi.org/10.5194/bg-11-4599-2014, 2014.

Roth, R., Ritz, S. P., and Joos, F.: Burial-nutrient feedbacks amplify the sensitivity of atmospheric carbon dioxide to changes in organic matter remineralisation, Earth Syst. Dyn., 5, 321–343, https://doi.org/10.5194/esd-5-321-2014, 2014.

Sabine, C. L., Feely, R. A., Gruber, N., Key, R. M., Lee, K., Bullister, J. L., Wanninkhof, R., Wong, C. S., Wallace, D. W. R., Tilbrook, B., Millero, F. J., Peng, T.-H., Kozyr, A., Ono, T., and Rios, A. F.: The Oceanic Sink for Anthropogenic CO_2, Science, 305, 367–371, https://doi.org/10.1126/science.1097403, 2004.

https://doi.org/10.5194/bg-2022-134
Preprint. Discussion started: 20 June 2022

Sanderson, B. M., Pendergrass, A. G., Koven, C. D., Brient, F., Booth, B. B. B., Fisher, R. A., and Knutti, R.: The potential for structural errors in emergent constraints, Earth Syst. Dyn., 12, 899–918, https://doi.org/10.5194/esd-12-899-2021, 2021.

Sarmiento, J. L. and Sundquist, E. T.: Revised budget for the oceanic uptake of anthropogenic carbon dioxide, Nature, 356, 589–593, https://doi.org/10.1038/356589a0, 1992.

Sarmiento, J. L., Orr, J. C., and Siegenthaler, U.: A perturbation simulation of CO_2 uptake in an ocean general circulation model, J. Geophys. Res. Ocean., 97, 3621–3645, https://doi.org/https://doi.org/10.1029/91JC02849, 1992.

Sarmiento, J. L., Le Quéré, C., and Pacala, S. W.: Limiting future atmospheric carbon dioxide, Global Biogeochem. Cycles, 9, 121–137, https://doi.org/https://doi.org/10.1029/94GB01779, 1995.

Sarmiento, J. L., Hughes, T. M. C., Stouffer, R. J., and Manabe, S.: Simulated response of the ocean carbon cycle to anthropogenic climate warming, Nature, 393, 245–249, https://doi.org/10.1038/30455, 1998.

Séférian, R., Gehlen, M., Bopp, L., Resplandy, L., Orr, J. C., Marti, O., Dunne, J. P., Christian, J. R., Doney, S. C., Ilyina, T., Lindsay, K., Halloran, P. R., Heinze, C., Segschneider, J., Tjiputra, J., Aumont, O., and Romanou, A.: Inconsistent strategies to spin up models in CMIP5: implications forocean biogeochemical model performance assessment, Geosci. Model Dev., 9, 1827–1851, https://doi.org/10.5194/gmd-9-1827-2016, 2016.

Séférian, R., Nabat, P., Michou, M., Saint-Martin, D., Voldoire, A., Colin, J., Decharme, B., Delire, C., Berthet, S., Chevallier, M., Sénési, S., Franchisteguy, L., Vial, J., Mallet, M., Joetzjer, E., Geoffroy, O., Guérémy, J.-F., Moine, M.-P., Msadek, R., Ribes, A., Rocher, M., Roehrig, R., Salas-y-Mélia, D., Sanchez, E., Terray, L., Valcke, S., Waldman, R., Aumont, O., Bopp, L., Deshayes, J., Éthé, C., and Madec, G.: Evaluation of CNRM Earth System Model, CNRM-ESM2-1: Role of Earth System Processes in Present-Day and Future Climate, J. Adv. Model. Earth Syst., 11, 4182–4227, https://doi.org/https://doi.org/10.1029/2019MS001791, 2019.

Sellar, A. A., Walton, J., Jones, C. G., Wood, R., Abraham, N. L., Andrejczuk, M., Andrews, M. B., Andrews, T., Archibald, A. T., de Mora, L., Dyson, H., Elkington, M., Ellis, R., Florek, P., Good, P., Gohar, L., Haddad, S., Hardiman, S. C., Hogan, E., Iwi, A., Jones, C. D., Johnson, B., Kelley, D. I., Kettleborough, J., Knight, J. R., Köhler, M. O., Kuhlbrodt, T., Liddicoat, S., Linova-Pavlova, I., Mizielinski, M. S., Morgenstern, O., Mulcahy, J., Neininger, E., O'Connor, F. M., Petrie, R., Ridley, J., Rioual, J.-C., Roberts, M., Robertson, E., Rumbold, S., Seddon, J., Shepherd, H., Shim, S., Stephens, A., Teixiera, J. C., Tang, Y., Williams, J., Wiltshire, A., and Griffiths, P. T.: Implementation of U.K. Earth System Models for CMIP6, J. Adv. Model. Earth Syst., 12, e2019MS001946, https://doi.org/https://doi.org/10.1029/2019MS001946, 2020.

https://doi.org/10.5194/bg-2022-134
Preprint. Discussion started: 20 June 2022

Steinacher, M., Joos, F., Frölicher, T. L., Bopp, L., Cadule, P., Cocco, V., Doney, S. C., Gehlen, M., Lindsay, K., Moore, J. K., Schneider, B., and Segschneider, J.: Projected 21st century decrease in marine productivity: a multi-model analysis, Biogeosciences, 7, 979–1005, https://doi.org/10.5194/bg-7-979-2010, 2010.

Stock, C. A., Dunne, J. P., Fan, S., Ginoux, P., John, J., Krasting, J. P., Laufkötter, C., Paulot, F., and Zadeh, N.: Ocean Biogeochemistry in GFDL's Earth System Model 4.1 and Its Response to Increasing Atmospheric CO_2, J. Adv. Model. Earth Syst., 12, https://doi.org/https://doi.org/10.1029/2019MS002043, 2020.

Talley, L. D.: Closure of the Global Overturning Circulation Through the Indian, Pacific, and Southern Oceans: Schematics and Transports, Oceanography, 26, 80–97, https://doi.org/10.5670/oceanog.2013.07, 2013.

Terhaar, J., Orr, J. C., Gehlen, M., Ethé, C., and Bopp, L.: Model constraints on the anthropogenic carbon budget of the Arctic Ocean, Biogeosciences, 16, 2343–2367, https://doi.org/10.5194/bg-16-2343-2019, 2019.

Terhaar, J., Kwiatkowski, L., and Bopp, L.: Emergent constraint on Arctic Ocean acidification in the twenty-first century, Nature, 582, 379–383, https://doi.org/10.1038/s41586-020-2360-3, 2020a.

Terhaar, J., Tanhua, T., Stöven, T., Orr, J. C., and Bopp, L.: Evaluation of Data-Based Estimates of Anthropogenic Carbon in the Arctic Ocean, J. Geophys. Res. Ocean., 125, 2020b.

Terhaar, J., Torres, O., Bourgeois, T., and Kwiatkowski, L.: Arctic Ocean acidification over the 21st century co-driven by anthropogenic carbon increases and freshening in the CMIP6 model ensemble, Biogeosciences, 18, 2221–2240, https://doi.org/10.5194/bg-18-2221-2021, 2021a.

Terhaar, J., Frölicher, T., and Joos, F.: Southern Ocean anthropogenic carbon sink constrained by sea surface salinity, Sci. Adv., 7, 5964–5992, https://doi.org/10.1126/sciadv.abd5964, 2021b.

Tjiputra, J. F., Schwinger, J., Bentsen, M., Morée, A. L., Gao, S., Bethke, I., Heinze, C., Goris, N., Gupta, A., He, Y.-C., Olivié, D., Seland, Ø., and Schulz, M.: Ocean biogeochemistry in the Norwegian Earth System Model version 2 (NorESM2), Geosci. Model Dev., 13, 2393–2431, https://doi.org/10.5194/gmd-13-2393-2020, 2020.

Wang, L., Huang, J., Luo, Y., and Zhao, Z.: Narrowing the spread in CMIP5 model projections of air-sea CO2 fluxes, Sci. Rep., 6, 37548, https://doi.org/10.1038/srep37548, 2016.

https://doi.org/10.5194/bg-2022-134
Preprint. Discussion started: 20 June 2022

Watson, A. J., Schuster, U., Shutler, J. D., Holding, T., Ashton, I. G. C., Landschützer, P., Woolf, D. K., and Goddijn-Murphy, L.: Revised estimates of ocean-atmosphere CO_2 flux are consistent with ocean carbon inventory, Nat. Commun., 11, 4422, https://doi.org/10.1038/s41467-020-18203-3, 2020.

Weiss, R. F.: Carbon dioxide in water and seawater: the solubility of a non-ideal gas, Mar. Chem., 2, 203–215, https://doi.org/https://doi.org/10.1016/0304-4203(74)90015-2, 1974.

Wenzel, S., Cox, P. M., Eyring, V., and Friedlingstein, P.: Emergent constraints on climate-carbon cycle feedbacks in the CMIP5 Earth system models, J. Geophys. Res. Biogeosciences, 119, 794–807, https://doi.org/https://doi.org/10.1002/2013JG002591, 2014.

Williamson, M. S., Thackeray, C. W., Cox, P. M., Hall, A., Huntingford, C., and Nijsse, F. J. M. M.: Emergent constraints on climate sensitivities, Rev. Mod. Phys., 93, 25004, https://doi.org/10.1103/RevModPhys.93.025004, 2021.

Winton, M., Griffies, S. M., Samuels, B. L., Sarmiento, J. L., and Frölicher, T. L.: Connecting Changing Ocean Circulation with Changing Climate, J. Clim., 26, 2268–2278, https://doi.org/10.1175/JCLI-D-12-00296.1, 2013.

Yukimoto, S., Kawai, H., Koshiro, T., Oshima, N., Yoshida, K., Urakawa, S., Tsujino, H., Deushi, M., Tanaka, T., Hosaka, M., Yabu, S., YOSHIMURA, H., SHINDO, E., MIZUTA, R., OBATA, A., ADACHI, Y., and ISHII, M.: The Meteorological Research Institute Earth System Model Version 2.0, MRI-ESM2.0: Description and Basic Evaluation of the Physical Component, J. Meteorol. Soc. Japan. Ser. II, 97, 931–965, https://doi.org/10.2151/jmsj.2019-051, 2019.

Zeng, J., Nojiri, Y., Landschützer, P., Telszewski, M., and Nakaoka, S.: A Global Surface Ocean fCO_2 Climatology Based on a Feed-Forward Neural Network, J. Atmos. Ocean. Technol., 31, 1838–1849, https://doi.org/10.1175/JTECH-D-13-00137.1, 2014.

Ziehn, T., Chamberlain, M. A., Law, R. M., Lenton, A., Bodman, R. W., Dix, M., Stevens, L., Wang, Y.-P., and Srbinovsky, J.: The Australian Earth System Model: ACCESS-ESM1.5, J. South. Hemisph. Earth Syst. Sci., 70, 193–214, 2020.

Zweng, M. M., Reagan, J. R., Seidov, D., Boyer, T. P., Locarnini, R. A., Garcia, H. E., Mishonov, A. V., Baranova, O. K., Weathers, K., Paver, C. R., and Smolyar, I.: World Ocean Atlas 2018, Volume 2: Salinity, 2018.